From THE DEPARTMENT OF CLINICAL NEUROSCIENCE
Karolinska Institutet, Stockholm, Sweden

Development of Novel Fluorine-18 labeled PET Radioligands for Monoamine Oxidase B (MAO-B)

Sangram Nag

Stockholm 2013

Published by Karolinska Institutet.

Printed by Univesity Service US-AB, Stockholm, Sweden.

ISBN 978-91-7549-150-9

ABSTRACT

Monoamine oxidases (MAO-A and MAO-B) are important enzymes regulating the levels of monoaminergic neurotransmitters. Selective and irreversible MAO-B inhibitors such as *L*-deprenyl and rasagiline are clinically used for the treatment of psychiatric and neurological disorders. Positron emission tomography (PET) is a non-invasive imaging technique which has widely been utilized to visualize the localization of MAO-B in monkey and human brains and thereby has been useful for studying neurodegenerative diseases and epilepsy. This thesis deals with the synthesis and evaluation of novel fluorine-18 labeled PET radioligands for detection of MAO-B activity.

The present thesis demonstrates that nine fluorinated propargyl amines were synthesized and tested for inhibition of MAO-B. In order to label those compounds with fluorine-18 seven chloro-precursors and two sulphamidate-precursors were also synthesized by multi step organic synthesis. Radiolabeling of six chloro-precursors with fluorine-18 was accomplished by a one-step nucleophilic substitution reaction. Radiolabeling of two sulphamidate-precursors with fluorine-18 was performed in two steps, compromising a nucleophilic substitution followed by the removal of the protecting group. The incorporation yield of the fluorination reactions varied from 40-70%. The radiochemical purity was >99% and the specific radioactivities were in a range of 190-240 GBq/μmol at the time of administration.

In vitro MAO inhibition and/or autoradiography (ARG) experiments demonstrated a high selectivity for MAO-B over MAO-A for five of the compounds namely [^{18}F]fluorodeprenyl, [^{18}F]fluororasagiline, [^{18}F]fluoro-*N*,4-dimethyl-*N*-(prop-2-ynyl) pentan-2-amine, [^{18}F]fluorodeprenyl-D_2 and [^{18}F]fluororasagiline-D_2. All five compounds were examined by PET and showed a high initial brain uptake in known MAO-B rich regions in cynomolgus monkey. [^{18}F]Fluorodeprenyl showed a kinetic behavior similar to [^{11}C]deprenyl where its fast irreversible binding to the enzyme renders the distribution of this radioligand in tissue limited by blood flow rather than the MAO-B enzyme concentration. [^{18}F]Fluororasagiline and [^{18}F]fluoro-*N*,4-dimethyl-*N*-(prop-2-ynyl)pentan-2-amine showed continuous increase of the radioactivity throughout the PET measurement that might be an indication of a blood-brain barrier penetrating radiometabolite which might in turn complicate a reliable quantification. Only [^{18}F]fluorodeprenyl-D_2 and [^{18}F]fluororasagiline-D_2 showed fast wash-out from the brain and less accumulation in cortical and sub-cortical regions. Radiometabolite studies demonstrated that both deuterated analogues were more stable measured in monkey plasma when compared to the non-deuterated analogues.

These results together suggest that both [^{18}F]fluorodeprenyl-D_2 and [^{18}F]fluororasagiline-D_2 may be improved PET radioligands and potential molecular imaging biomarker candidates for PET studies in neuroinflammation and neurodegeneration, accompanied with astrocyte activation.

You can't cross the sea merely by standing and staring at the water.

Rabindranath Tagore

To Jolly, Leeba & My Parents

LIST OF PUBLICATIONS

I. Nag S., Lehmann L., Heinrich T., Thiele A., Kettschau G., Nakao R., Gulyas B. and Halldin C. Synthesis of three novel fluorine-18 labeled analogues of *L*-deprenyl for positron emission tomography (PET) studies of monoamine oxidase B (MAO-B). *Journal of Medicinal Chemistry* **2011**, 54, 7023-7029.

II. Nag S., Varrone A., Toth M., Thiele A., Kettschau G., Heinrich T., Lehmann L. and Halldin C. *In vivo* evaluation in cynomolgus monkey brain and metabolism of [^{18}F]fluorodeprenyl: A new MAO-B pet radioligand. *Synapse* **2012**, 66, 323-330.

III. Nag S., Lehmann L., Kettschau G., Heinrich T., Thiele A., Varrone A., Gulyas B. and Halldin C. Synthesis and evaluation of [^{18}F]fluororasagiline, a novel positron emission tomography (PET) radioligand for monoamine oxidase B (MAO-B). *Bioorganic & Medicinal Chemistry* **2012**, 20, 3065-3071.

IV. Nag S., Kettschau G., Heinrich T., Varrone A., Lehmann L., Gulyas B., Thiele A., Keller E. and Halldin C. Synthesis and biological evaluation of novel propargyl amines as potential fluorine-18 labeled radioligands for detection of MAO-B activity. *Bioorganic & Medicinal Chemistry* **2013,** 21, 186-195.

V. Nag S., Lehmann L., Kettschau G., Toth M., Heinrich T., Thiele A., Varrone A. and Halldin C. Synthesis and PET evaluation of a novel fluorine-18 labeled deuterated fluorodeprenyl ([^{18}F]fluorodeprenyl-D_2) radioligand to study MAO-B Activity. Submitted.

VI. Nag S., Lehmann L., Kettschau G., Toth M., Heinrich T., Thiele A., Varrone A. and Halldin C. Development of a novel fluorine-18 labeled deuterated fluororasagiline ([^{18}F]fluororasagiline-D_2) radioligand for PET studies of monoamine oxidase B (MAO-B). Submitted.

CONTENTS

LIST OF ABBREVIATIONS

^{11}C	Radioactive, neutron deficient isotope of carbon
^{13}N	Radioactive, neutron deficient isotope of nitrogen
^{15}O	Radioactive, neutron deficient isotope of oxygen
^{18}F	Radioactive, neutron deficient isotope of fluorine
^{68}Ga	Radioactive, neutron deficient isotope of gallium
AD	Alzheimer's disease
ARG	Autoradiography
BBB	Blood brain barrier
B_{max}	Receptor density
BP	Binding potential
Bq	Bequerel, SI derived unit of radioactivity
CNS	Central nervous system
CT	Computed tomography
Cyclotron	Particle accelerator
DAST	Diethylaminosulfur trifluride
DMF	Dimethylformamide
DMSO	Dimethyl sulfoxide
FAD	Flavin adenine dinucleotide
HPLC	High performance liquid chromatography
HRRT	High resolution research tomography
i.v.	Intravenous
IC	Inhibitory concentration
ID	Injected dose
In vitro	"in flask" i.e. in the test tube
In vivo	"in life" i.e. in the organism
K_d	Dissociation constant
Kryptofix	4,7,13,16,21,24-hexaoxa-1,10-diazabicyclo-[8.8.8] hexacosane-$K_{2.2.2}$
LAD	Lithium aluminium deutride
LAH	Lithium aluminium hydride
LC-MS	Liquid chromatography-mass spectrometry
Lipophilic	Non-polar, tendency to not dissolve in water
LogP	Logarithm of partition coefficient
MAO	Monoamine oxidase
MeCN	Acetonitrile
MeV	Mega electron volt
MRI	Magnetic resonance imaging
NMR	Nuclear magnetic resonence
NMRI	Naval medical research institute
p.i.	Post injection
PBS	Phosphate buffered solution

PD	Parkinson's disease
PET	Positron emission tomography
ROI	Region of interest
RT	Room temperature
SA	Specific radioactivity
S_N2	Bimolecular nucleophilic substitution
$T_{1/2}$	Half-life
TAC	Time activity curve
THF	Tetrahydrofuran
UPLC	Ultra performance liquid chromatography
UV	Ultraviolet

1 INTRODUCTION

1.1 POSITRON EMISSION TOMOGRAPHY (PET)

The development of science has made it possible to track and quantify the spatial distribution patterns and dynamics of radioactivity in a living organism over time. Positron emission tomography (PET) is one of the most powerful technologies for this purpose which utilizes positron-emitting nuclides as the radioactive source[1-4]. Even though PET is a relatively recent technology, the principle has been understood for half a century. The first commercial PET scanners were developed in the late 1960's which were using analogue electronics to generate tomographic images. In the late 1970's more sensitive detectors and tomographic capabilities began to appear and by the mid-1990's, PET became an important medical diagnostic tracer technique based on the detection of positron annihilation radiation and the subsequent processing of raw data into an image[5, 6]. It allows the investigation of bio-chemical transformations of drugs or other molecules in living systems and thereby offers possibilities to study physiology, molecular biology, energy metabolism, and drug-receptor or drug-enzyme interactions. This also allows the methods, knowledge, and interpretation of results from tracer kinetic assays used in the basic biological sciences to be applied to humans by the quantitative measurement abilities of the PET system. PET is therefore rapidly becoming a major molecular imaging modality with several applications in oncology[7], neuroscience[8, 9] and cardiovascular imaging[10].

The reason why PET is so successful is that it enables to study the physiological parameters at the chemical and molecular level. Conventional imaging techniques such as X-ray, CT scans, and magnetic resonance imaging (MRI) provide mainly anatomical information. PET can detect the presence of chemical and metabolic changes in disease states, such as cancer, independently of the anatomic or structural changes detected by conventional imaging. In oncology PET can help in differentiating benign from malignant processes based on differences in biological activity. In addition, whole body imaging with PET provides a means to examine all the organ systems in the entire body for both primary and metastatic diseases in one procedure.

Moreover PET is important not only from the diagnostic point of view; it can also play an important role in the discovery and development of new drugs[11-16]. The drug development process is a time consuming and expensive process and unfortunately most of the candidate drugs fail in the final step i.e. in clinical studies. It is possible to perform clinical studies earlier using PET microdosing concept[17] in receptor occupancy studies and thereby to speed up the drug development process.

1.2 HOW DOES PET WORK

The transfer of tracer methods from the basic biological sciences to humans with PET is made possible by the unique nature of the radionuclides used in PET to label compounds such as ^{11}C ($t_{1/2}$ = 20.4 min), ^{18}F ($t_{1/2}$ = 109.77 min), ^{15}O ($t_{1/2}$ = 2.04 min), and ^{13}N ($t_{1/2}$ = 9.97 min). These are the radioactive forms of the natural elements such as ^{12}C, ^{19}F, ^{16}O and ^{14}N that emit radiation which will pass through the body for external detection. Natural substrates, substrate analogues, and drugs are labeled with these radio isotopes without altering their chemical or biological properties. As a consequence, a very small amount of the radiolabeled compound can be administered, which allows biochemical processes to be studied *in vivo* over time without perturbing the system. Due to the short half-life of the radionuclide, radiolabeling, purification, quality control and administration should be accomplished within a very short time. Therefore, the radionuclide is incorporated as late as possible in the synthetic route. The short half-life of the radionuclides enable a sufficient amount of statistical data to be collected during the PET scan while keeping the radiation dose to a minimum.

The nuclei of the positron-emitting radionuclides are neutron-deficient and decay by the conversion of a proton into a neutron by the emission of a positron (β^+) and a neutrino (υ_e). Carbon-11 or fluorine-18 has a short half-life and positron emission accounts for 99% of its decay.

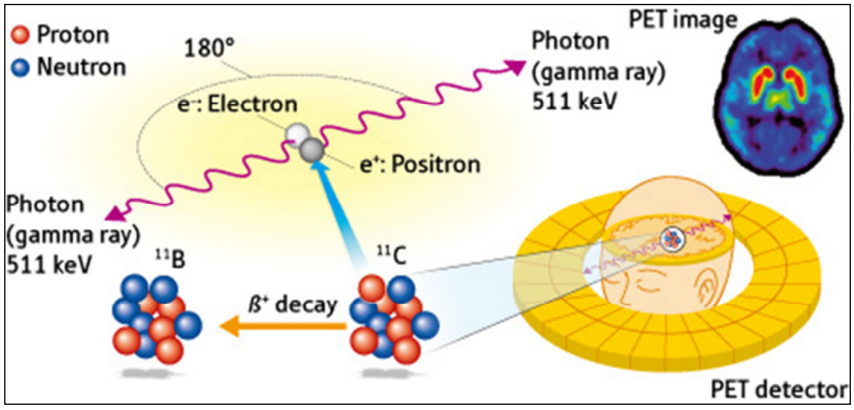

Figure 1. Principle of positron emission tomography (PET) exemplified by ^{11}C to ^{11}B decay[18].

The positron (β+) can travel up to a few millimeters in wet tissue before encountering its antiparticle, an electron (e-), causing an annihilation that generates two high-energy (511 keV) gamma ray photons, which are emitted in essentially opposite directions (Figure 1). The total positron and negatron energy is therefore 1.22 MeV, the sum of their equal rest mass energies (Eo=511 keV=0.511 MeV), and their total momentum is zero. PET is based on the annihilation coincidence detection (ACD) of the two collinear 511 keV rays. The photons are detected in coincidence as they reach the scintillators, creating a burst of light that in turn is amplified by photomultipliers, giving rise to an electrical signal that can be further processed by computing program. Only signals that

are detected in pairs within a few nanoseconds are considered to originate from the same radioactive decay; the single photon detections that result from scattering are ignored. The detectors in the PET camera are arranged in a ring around the object under study, allowing the location of the decay to be determined.

1.3 DEVELOPMENT OF PET RADIOLIGANDS

Development of PET radioligands specific for receptors or enzymes has made it possible to evaluate the density and pharmacological action of receptors or enzymes in the brain, in addition to the receptor occupancy of therapeutic drugs. The success of a PET radioligand largely depends on its use in the applied experiment. Although the development of PET radioligands has been carried out for more than three decades, at present only relatively few established radioligands are available for a small number of targets. The development of new PET radioligands is needed together with the increasing use of PET in medical and biomedical research. Advancement of radiochemistry is needed in order to meet the growing demand for labeled potential PET radioligands. The development of a new radioligand is a complex and multidisciplinary field which is associated with physics, radiochemistry, medicinal chemistry, biology, pharmacology, drug metabolism, mathematics and regulatory affairs.

A successful radioligand for CNS PET studies must provide information which is suitable for quantitative analysis of the target. The outcome result of a PET experiment is usually the binding potential (BP) and a reliable quantitative analysis. In order to acquire those a radioligand is required to have some important properties[12, 19, 20,21, 22] such as a suitable binding affinity, selectivity and specificity, lipophilicity and brain penetration, specific radioactivity (SA), radiolabeling and metabolism. The most common obstacle in developing a new PET radioligand is the relatively small window of appropriate combinations of the above mentioned parameters.

1.3.1 Binding affinity

Binding affinity is expressed as the inverse equilibrium dissociation constant (K_d). Binding affinity is an important requirement for a radioligand to be successful because of the concentration of binding sites (B_{max}) in the region of interest. A typically successful radioligand has subnanomolar affinity to the target of interest and B_{max} should exceed the K_d of radioligands for good image contrast. A ratio of 5-10 between B_{max} and K_d can be used as initial parameters for developing new PET radioligands[23, 24]. A low concentration of binding sites means the radioligand should have a high binding affinity. Quantification of a reversibly-binding ligand is generally preferable over an irreversible one[25].

1.3.2 Selectivity and specificity

The success of a PET radioligand is highly dependent on its appropriate pharmacodynamics properties, such as selectivity and specificity for the target. Selectivity and specificity of the radioligand for the binding site is a key factor that affects the degree of nonspecific binding which is a major challenge in the development of radioligands. Nonspecific binding occurs when the radioligand binds with a molecular target or tissue other than the site of interest which is a major challenge in the development of new radioligands and is often considered as the reason for the high failure rate of new radioligands[26].

1.3.3 Lipophilicity and brain penetration

Lipophilicity is an important physicochemical property which influences a radioligand´s absorption, distribution, metabolism and elimination. It is expressed as the partition ratio of a compound in octanol/water or as the logP or logD value. Lipophilicity can be calculated theoretically or measured experimentally. The partition coefficient, P, is used for the neutral compound, whereas the distribution coefficient, D, is used for the sum of all micro-species (μ-species) for ionisable compounds. The distribution coefficient, D, is pH-dependent.

$$Partition\ coefficient\ P = ([Compound]_{octanol})/([Compound]_{water})$$

$$Distribution\ coefficient\ D = (\sum[\mu - species]_{octanol})/(\sum[\mu - species]_{water})$$

Lipophilicity is the most important factor for a radioligand´s capacity to cross the lipid membranes which is essential for targets in the CNS[22, 27, 28]. The extent of the radioligand´s specific to nonspecific binding ratios can also be affected by lipophilicity. Furthermore high lipophilicity leads to high protein binding and reduces the delivery of the radioligand to the specific sites[29]. On the other hand radioligands with low lipophilicity have higher water solubility, faster clearance through the kidneys and low blood-brain barrier (BBB) penetration. However, in the brain, a moderate lipophilicity and high affinity are required to achieve high ratios of specific to nonspecific binding[29]. For a molecule to cross the BBB, relatively small molecular weight (<600 daltons) and moderate lipophilicity are required. The suitable logP for radioligand to cross the BBB is in between 1.5 and 3.5[30]. BBB is well equipped with efflux pump P-glycoprotein (P-gp) which functions to repel many unwanted or xenobiotic compounds. Therefore, radioligands which are substrates for P-gp are highly inhibited at the BBB and are unable to reach the target[31, 32]. In general, substrate behavior for P-gp is promoted by high lipophilicity, positive charge at pH 7.4 and multiple aromatic groups[33].

1.3.4 Specific radioactivity (SA)

The term "specific radioactivity" (SA) is defined as the amount of radioactivity or the decay rate of a particular radionuclide per unit mass of the radionuclide which is

generally expressed as the radioactivity of the labeled compound divided by the molar amount of the compound (Bq/mol). SA is an important parameter to be considered for the development of PET radioligands. A high SA is necessary due to many biological factors such as limited amount of receptors, high binding affinity to the receptor, and risk of inducing pharmacological side effects. In particular, due to competition with the labeled compound for the same receptor, the presence of unlabeled compound may have a negative effect on the concentration of radioactivity in the target tissue. Hence, a high SA might be critical for providing a sufficient contrast in PET images between the target tissue and its surroundings. For example, in order to visualize extrastriatal D2 receptors by the dopamine D2 receptor radioligand [^{11}C]FLB 457 with picomolar binding affinity of 20 pmol/L, a SA higher than 110 GBq/µmol is required for data quantification[34]. The maximal theoretical SA can be calculated from the following equation:

$$SA = \lambda N, \ (\lambda = \frac{ln2}{T_{\frac{1}{2}}})$$

(λ = decay constant, N = Avogadro constant, $T_{\frac{1}{2}}$ = the half-life of the radionuclide)

Theoretical SA only depends on the half-life of the radionuclide and not on time. The maximal theoretical SA for ^{18}F is 6.3 × 104 GBq/µmol[35, 36]. The SA obtained in a labeling experiment is usually much lower than the theoretical value due to isotopic dilution which means that SA will be a function of time and exponentially decline with the half-life of the radionuclide.

$$SA\ (t) = \frac{A(t)e^{-\left(\frac{ln2}{T_{\frac{1}{2}}}\right)t}}{m}$$

Where A(t) = radioactivity at the time of measurement, t = time after radioactivity measurement, m = mass of the compound.

1.3.5 Radiolabeling and metabolism

The radiolabeling of radiopharmaceuticals to be applied in PET is a complicated and extremely challenging process. The main challenge of using short-lived PET radioisotopes is their short half-life which imposes severe time restrictions. Therefore, PET radiolabeling procedures are usually limited to one or two distinct chemical steps with the introduction of the PET radioisotope as late in the radiosynthesis as possible. Recent development of the micro-reactor technology for radiosynthesis has some major advantages such as purer products, higher yields, shorter reaction time than for corresponding batch reactions, and more benign reaction conditions[37, 38]. The labeling position is also a key consideration, and can pose mainly two significant challenges, such as: i) is it synthetically viable and ii) is it metabolically stable. [^{11}C]CO can play

an important role for labeling with carbon-11 at different position due to the broad range of labelling chemistry available using [^{11}C]CO[39, 40].

One of the main reasons for failure of PET radioligands for CNS is if a radiometabolite enters the brain. PET experiments cannot differentiate between emitted gamma rays by the parent radioligand and emitted gamma rays by a radiolabeled metabolite. If a radiolabeled compound is rapidly metabolized, the radiometabolites may affect the acquisition of data and the quantitative parameters derived from[41, 42] a PET study. Labeling a molecule in different positions can provide important *in vivo* metabolic information which is useful in determining the best labeling position. One example is the serotonin 5-HT$_{1A}$ receptor radioligand [^{11}C]WAY100635[43].

1.4 MONOAMINE OXIDASE (MAO)

In 1928 an enzyme called tyramine oxidase that catalyzed the oxidative deamination of tyramine was first isolated by Mary Hare[44]. Later it was shown by Blaschko and co-workers that this same enzyme also possessed the property to oxidize catecholamines[45]. To reflect the more general reactivity of this enzyme, a general name monoamine oxidase (MAO) was given by Zeller in 1938[46]. This enzyme is mainly found as an integral protein in the outer membrane of mitochondria in most cell types in the body, neuronal and non-neuronal cells in the brain and in peripheral organs[47]. Two isoforms of the MAO enzyme were found and called "MAO Type A" (MAO-A) and "MAO Type B" (MAO-B) according to their biochemical and pharmacological properties[48]. In general, MAO-A selectively oxidizes the "neurotransmitter" monoamines such as epinephrine, norepinephrine and 5-hydroxytryptamine while MAO-B selectively oxidizes the monoamines such as benzylamine, phenylethylamine, methylhistamine, *N*-acetylputrescine, MPTP, *N*-phenylamine, octylamine. Both MAO-A and MAO-B oxidize tyramine, tryptamine, kynuramine, 3-methoxytyramine and dopamine[49]. MAO-B catalyzes the oxidative deamination of catecholamine neurotransmitters, generating hydrogen peroxide which can form highly reactive oxygen species due to the presence of hydroxyl radicals. In Alzheimer´s disease (AD) increased oxidative stress is attributed to the aberrant generation of reactive oxygen species, leading to neurodegeneration[50].

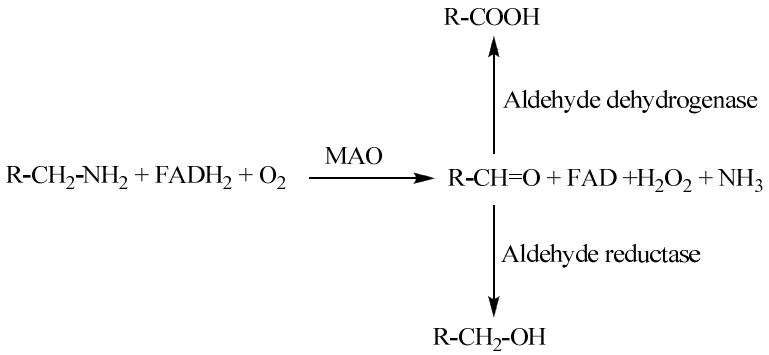

Scheme 1. Schematic representation of the oxidative deamination of monoamines to the corresponding aldehydes by MAO

In humans MAO-A is mostly expressed in the placenta, the adipose tissue, the thyroid gland and the lung, whereas its expression in various parts of the brain is rather low. In contrast, MAO-B is dominantly expressed in various parts of the CNS such as the striatum, the hypothalamus, the prefrontal cortex, the amygdala and the spinal cord. Furthermore, the uterus, the kidney, the liver and the heart are also rich sources for MAO-B[51]. In the CNS, MAO-A is predominantly found in catecholaminergic neurons, whereas MAO-B is more abundant in serotonergic and histaminergic neurons as well as in astroglial cells[52-54]. In the human brain MAO-B constitutes up to ~70% of total brain MAO activity[55-57]. Cerebral MAO-B level increases with age and a further up regulated in the brains of e.g. AD patients. Because of its central role in neurotransmitters metabolism, MAO-B represents an attractive target in the pharmacological therapy of neurodegenerative diseases such as AD[55,58], Parkinson's disease (PD)[59], depression[60] as well as social anxiety[61].

Both MAO isoforms differ in their inhibition properties and can be inhibited depending upon the chemical structure or the relative concentrations of the inhibitor. MAO inhibitors were employed clinically in the 1950s. MAO-A is selectively inhibited by e.g. pirlindole and clorgyline which have found to be highly effective in the treatment of depression[62]. On the other hand MAO-B inhibitors are applied for the treatment of PD[63] as well as for depression[64]. MAO-B inhibitors can be distinguished into two classes such as reversible inhibitors and irreversible inhibitors[65].

Reversible MAO-B inhibitors are structurally related to MAO-B substrates, and bind to the active site of the enzyme and are metabolized relatively slowly. On the other hand irreversible or "suicide" inhibitors initially bind to MAO-B in a reversible fashion, are then are oxidized by the enzyme to the active inhibitor, which covalently binds to the enzyme via the flavin adenine dinucleotide (FAD) cofactor, thus rendering it permanently unavailable for amine metabolism[66]. *L*-deprenyl was the first compound identified as an irreversible MAO-B inhibitor and has 150-folds more potency over its *D*-isomer[67, 68]. More recently investigated MAO-B inhibitors such as rasagiline[69], and mofegiline[70] show irreversible binding properties whereas lazabemide[71-73] shows a reversible binding property and milacemide[74] shows partially reversible binding property.

1.5 MAO-B PET RADIOLIGANDS

The PET technique has been applied as an useful tool for imaging brain MAO-B activity in humans for studying neurodegenerative diseases[75] and epilepsy[76]. Till now a number of selective and reversible or irreversible radioligands have been developed (Figure 2) in order to study MAO-B activity and density by PET[77-79]. For example [^{11}C]deprenyl[80, 81], [^{11}C]pargyline[82], [^{11}C]deprenyl-D_2[83, 84], [^{11}C]MD230254[85], *DL*-4-[^{18}F]fluorodeprenyl[86] and 6-[^{18}F]fluoro-*N*-methyl-*N*-(prop-2-yn-1-yl)-hexan-1-amine[87] showed irreversible binding properties for imaging MAO-B, whereas [^{11}C]SL25.1188[88] and [^{18}F]Ro43-0463[89, 90] indicated more reversible binding properties. A reversible

binding MAO-B radioligand might have advantages over the irreversible one due to its faster wash out from the brain. Among those radioligands only carbon-11 labeled compounds such as [^{11}C]deprenyl[81] and [^{11}C]deprenyl-D_2[84, 91] were demonstrated as useful PET radioligands for assessing MAO-B in the human brain. MAO-B substrate *N*,*N*-dimethylphenylethylamine (DMPA) was labeled with carbon-11 at two different positions and used to measure the MAO-B activity in monkey brain[92]. So far no successful fluorine-18 labeled PET radioligand has been validated for clinical use. Therefore, there has been much interest in the development of fluorine-18 labeled MAO-B inhibitors as biological probes to map MAO-B activity.

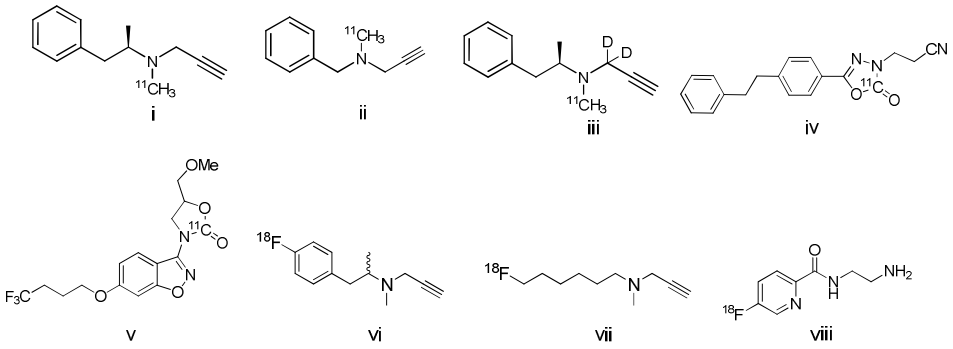

Figure 2. Structures of MAO-B PET radioligands: i) [^{11}C]deprenyl, ii) [^{11}C]pargyline, iii) [^{11}C]deprenyl-D_2, iv) [^{11}C]SL25.1188, v) [^{11}C]MD230254, vi) *DL*-4-[^{18}F]fluorodeprenyl and vii) 6-[^{18}F]fluoro-*N*-methyl-*N*-(prop-2-yn-1-yl)- hexan-1-amine, viii) [^{18}F]Ro 43-0463.

1.6 STRATEGIES OF ^{18}F-LABELING

Fluorine is widely introduced in pharmaceutical compounds despite an unusual natural occurrence in biological molecules[93]. Although the introduction of a fluorine atom in a molecule generally modifies the physical and biological properties[94], a large number of molecules exist where hydrogen was replaced by fluorine and the new molecules retained comparable properties[95]. [^{18}F]Fluoride is one of the most widely used radionuclides in PET. Its convenient half-life ($T_{1/2}$ = 110 min), β^+ emitting decay mode, low positron energy (0,63 MeV), low radiation dose, short ranges in tissue and the possibility to distribute to the site that doesn't have onsite cyclotron support it to be a suitable radionuclide for use in PET. [^{18}F]Fluoride can be introduced to the radioligand by both nucleophilic and by electrophilic substitution. However, only nucleophilic [^{18}F]fluoride fluorination was used in the work described in this thesis.

1.6.1 Electrophilic radiofluorination

For electrophilic radiofluorination reactions, [^{18}F]fluorine gas ([^{18}F]F_2) is used as electrophile. [^{18}F]F_2 gas is produced via the nuclear reaction ^{20}Ne(d,α)^{18}F and is liberated from the cyclotron with [^{19}F]F_2[96]. As a result, the ^{18}F/^{19}F ratio is quantified as SA. Therefore, SA of electrophilic [^{18}F]fluorine is in general low and not optimal for

synthesizing high SA ^{18}F-labeled radiopharmaceuticals. When [^{18}F]F_2 is used for electrophilic substitution, the maximum achievable radiochemical yield is 50% because only one of the fluorine atoms in [^{18}F]F_2 is labeled with [^{18}F]F.

However, in 1997, Solin *et al.* developed a method to generate [^{18}F]F_2 with a higher SA upto 55 GBq/µmol than what is common for [^{18}F]F_2 upto 2 GBq/µmol[97]. In this approach ^{18}F-labeled methyl fluoride ([^{18}F]CH_3F) is synthesized from [^{18}F]F^- aq(-). Then [^{18}F]CH_3F is flushed with neon gas in a quartz discharged chamber containing a variable amount of F_2 where an exchange of F-18 for F-19 takes place. Applying this method, recently, Gouverneur succeeded in synthesizing [^{18}F]F-TEDA, an electrophilic ^{18}F-fluorination reagent more useful and selective than [^{18}F]F_2[98]. Generally, [^{18}F]F_2 is converted into less reactive and more selective [^{18}F]fluorination agents[99].

Historically most early ^{18}F labeled tracers were synthesized via the electrophilic path way such as [^{18}F]FDG[100] and then nucleophilic pathways were developed to obtain higher radiochemical yield with higher specific SA[101]. Despite the lower radiochemical yield and lower SA, electrophilic fluorination is still used today in the production of PET radioligands, e.g. [^{18}F]F-DOPA[102]. Electrophilic fluorination was not considered in the current thesis work.

1.6.2 Nucleophilic radiofluorination

Nucleophilic substitution is a chemical reaction involving the addition of a nucleophilic molecule/atom into a molecule with a leaving group. As a result, the nucleophilic molecule forms a covalent bond with the parent molecule by displacing the leaving group via S_N2 mechanism. In nucleophilic radiofluorination, [^{18}F]fluoride ion is the nucleophile.

The [^{18}F]fluoride ion is prepared by the nuclear reaction $^{18}O(p,n)^{18}F$ in aqueous environment. In an aqueous environment, negatively charged ions must be accompanied by positively charged counter ions. [^{18}F]Fluoride is washed out from the cyclotron target with traces of metal ions (counter ions) from the surface of the target. Nucleophilic [^{18}F]F^- fluorination is also very sensitive to the presence of metal-ion traces formed by irradiation of the target[103]. Therefore, [^{18}F]fluoride ion is isolated by passing through a light QMA Sep-Pak column where [^{18}F]fluoride is retained by an ion-exchange reaction and allow the ^{18}O-water as well as the metal ions to flow through. The retained [^{18}F]fluoride ion is then eluted with an acetonitrile solution of Kryptofix and potassium carbonate [104, 105]. Potassium carbonate and Kryptofix $_{2.2.2}$ are commonly used as counter ion and a phase-transfer catalyst.

Fluorine has high hydration energy and the fluoride ion is a poor nucleophile in aqueous media. Therefore nucleophilic substitution reactions involving [^{18}F]fluoride ion requires strict exclusion of water. The advantage of using acetonitrile as the eluting solvent is that it forms an azeotropic mixture with water. Evaporation of the acetonitrile

in a nitrogen atmosphere will remove any residual ^{18}O-water[105] simultaneously. The classical "rule" is that increased dryness will increase the reactivity of the [^{18}F]fluoride ion. There are however numerous aliphatic reactions, that withstand relatively large amounts of water without influencing the radiochemical yield (RCY)[106]. Nucleophilic substitution with [^{18}F]fluoride generally occurs by heating the dried residue of the K^+[^{18}F]fluoride-K_{222} complex with the precursor in a polar aprotic solvent such as acetonitrile, DMSO and DMF[107]. Currently, the use of certain polar protic solvents has been applied successfully in several examples[108-110].

In general nucleophilic substitution with [^{18}F]fluoride is divided into aliphatic and aromatic substitution reactions. The aliphatic substitution reactions proceeds via a S_N2 mechanism, using common leaving groups such as sulfonic acid esters (e.g. triflates, tosylates , mesylates or sulphamidate) or halides (Cl, Br or I). The choice of leaving group depends mainly on the stability of the precursors, the purification of the ^{18}F-labeled product and the potential for formation of byproducts[111].

Nucleophilic aromatic substitution with [^{18}F]fluoride is the synthesis of aryl [^{18}F]fluorides[112]. A prerequisite, is that the aromatic ring needs to be activated by the presence of one or more electron-withdrawing groups such as nitro-, cyano-, carbonyl-, positioned at ortho- or para- to the leaving group[112]. There are several possible alternatives for leaving groups but mostly a halogen, nitro or trialkylammonium group is substituted[113, 114]. A recent study shows that the diphenyliodonium (Ar-I^+-Ar') group has an advantage over the presence of unnecessary electron withdrawing groups on the ring, but problems are associated with undesired radioactive byproducts[115].

A simple isotopic substitution, ^{18}F for ^{19}F, shows in general high radiochemical yield. However, the lower specific activity from these isotopic substitutions makes this process less practiced.

All the fluorination reactions described in this thesis proceeded via S_N2 mechanism in which either a chloride or a sulphamidate group was substituted by [^{18}F]F^- followed in some cases by the removal of a protecting group.

2 AIMS

The overall aim of this thesis was to develop fluorine-18 labeled PET radioligands for imaging MAO-B.

The following specific aims were set to meet the main objective:

(i) To synthesize the precursors and reference standards

(ii) To develop efficient synthetic methods for labeling the target compounds with fluorine-18

(iii) To evaluate their binding to MAO-B *in vitro* and *in vivo* as well as to study the metabolic stability of the parent compounds measured in monkey blood plasma.

3 EXPERIMENTALS AND METHODS

A brief summary of the general experimental and methods used during this thesis work are described here.

3.1 CHEMISTRY

3.1.1 Instrumentation and purification

^{1}H NMR spectra were referenced internally on $CDCl_3$ ($\delta^{1}H$ 7.26) and ^{13}C NMR spectra were referenced internally on $CDCl_3$ ($\delta^{13}C$ 77.20). Liquid chromatographic analysis (LC) was performed with a Merck-Hitachi gradient pump and a Merck-Hitachi, L-4000 variable wavelength UV-detector. A µ-Bondapak C-18 column (300 X 7.8 mm, 10 µm; Waters instruments) was used with a flow of 2 mL/minutes. LC-MS was performed using a Waters Quattra-ToF Premier micro mass spectrometer, or Waters SQD 3001 single quadrupole mass spectrometer, coupled to Waters Acquity UPLC instruments. The ionization mode used was electro spray positive ionization (ESI+). Analytical TLC was carried out on 0.25 mm silica gel plates.

Purification was not necessary in some cases and for certain cases, the compounds were purified by crystallization or distillation. In other cases, the compounds were purified by flash column chromatography, using prepacked silica gel cartridges, e.g. from Separtis such as Isolute® Flash silica gel or Isolute® Flash NH_2 silica gel in combination with e.g. a FlashMaster II autopurifier (Argonaut/Biotage) and eluents such as gradients of hexane/EtOAc or pentane/diethyl ether. In some cases, the compounds were purified by preparative HPLC using a Waters auto purifier equipped with a diode array detector and/or on-line electrospray ionization mass spectrometer in combination with a suitable prepacked reverse phase column and eluents such as gradients of water and acetonitrile which may contain additives such as trifluoroacetic acid or aqueous ammonia.

All solvents and chemicals were obtained from commercial sources and used without further purification. Purity of all synthesized compounds was ≥95% and was determined by NMR, HPLC, UPLC and LC-MS.

3.1.2 General procedures for the synthesis

3.1.2.1 Reduction by lithium aluminium hydride or lithium aluminium deuteride

To a solution of starting material in dry THF, lithium aluminium hydride (LAH) or lithium aluminium deutride (LAD) (1M in THF) was added dropwise at -5°C. The reaction mixture was refluxed overnight and cooled to -5°C. Unreacted LAH was quenched with aq NaOH and the mixture was stirred at RT for additional 30 minutes.

The reaction mixture was filtered and the filter cake was washed with diethyl ether (50 mL). The filtrate was dried over $MgSO_4$ and solvent was removed under reduced pressure to obtain the final product. The product was analyzed by NMR and LC-MS and used in the next step without further purification.

3.1.2.2 Synthesis of intermediate propargyl amine

To a solution of crude secondary amine in dry THF, K_2CO_3 was added and stirred at RT for 30 minutes. To the stirred solution propargyl bromide was added dropwise and the reaction mixture was stirred overnight at room temperature (RT), diluted with water and extracted with CH_2Cl_2 (3 x 50 mL). The organic phase was separated followed by washing with saturated $NaHCO_3$ and brine. Collected organic phases were dried over $MgSO_4$ and filtered. The solvent was removed under reduced pressure to obtain the crude product as light yellow oil. The crude product was purified by silica-gel column chromatography. Final product was obtained as oil and was analyzed by NMR, HPLC and LC-MS.

3.1.2.3 Synthesis of (1,1-$^2H_2$)3-bromoprop-1-yne (deuterated propargyl bromide)

To the stirred solution of (1,1-$^2H_2$)prop-2-yn-1-ol in dichloromethane at -5°C under nitrogen, phosphorus tribromide (PBr_3) was added dropwise. The solution was stirred at that temperature for one hour followed by stirring additional three hours at RT. The reaction mixture was quenched at 0°C with H_2O. The organic layer was washed successively with saturated $NaHCO_3$ and H_2O and dried over $MgSO_4$. The solvent was allowed to evaporate carefully and the final product was obtained as colorless oil and was analyzed by NMR. The product was considered pure enough for the next step without further purification.

3.1.2.4 Synthesis of chloroprecursors

A mixture of intermediate propargyl amine and triethyl amine or pyridine in THF was stirred at RT for 30 minutes. To the stirred mixture mesyl chloride was added drop wise at -7°C and the reaction mixture was stirred at RT for additional 30 minutes. Saturated aqueous Na_2CO_3 solution was added and stirred for an additional 30 minutes. The organic layer was partitioned between CH_2Cl_2 and water. The organic phase was separated and washed with saturated $NaHCO_3$ solution and brine followed by dried over $MgSO_4$ and filtered. The solvent was removed under reduced pressure to obtain the crude product as light yellow oil. The crude product was purified by silica-gel column chromatography and final product was obtained as light yellow oil. The product was analyzed by NMR, HPLC and LC-MS. The final product was a mixture of two isomers.

3.1.2.5 Synthesis of fluorinated reference standards

To the stirred solution of propargyl aminoalcohol in dichloromethane, diethylamino sulfurtrifluoride (DAST) was added dropwise at -5°C and the reaction mixture was stirred for 20 minutes at the same temperature. Saturated Na_2CO_3 solution was added to quench unreacted DAST. The organic layer was partitioned between CH_2Cl_2 and water. The organic phase was separated and washed with brine and dried over $MgSO_4$ followed by filtration. The solvent was removed under reduced pressure to obtain the crude product as light yellow oil. The crude product was purified by silica-gel column chromatography and gave the final product. The product was analyzed by NMR, HPLC and LC-MS.

3.1.2.6 Synthesis of fluororasagiline

To a solution of intermediate sulphamide in a mixture of DMF and *tert*-butanol, cesium fluoride was added, and the resulting mixture was stirred at RT for 60 hours. All volatiles were then removed *in vacuo*, followed by addition of 4N hydrochloric acid and ethanol to the residue. The resulting mixture was stirred at 80°C for 1.5 hours, allowed to cool to RT, and then partitioned between EtOAc and saturated aqueous Na_2CO_3. The aqueous layer was extracted with ethyl acetate and the combined organic layers were washed with brine, dried over $MgSO_4$, and allowed to evaporate. The residue was purified by column chromatography on silica gel (EtOAc in hexane 0% → 40%) to give the desired product. Highly purified material was obtained by short-path distillation of an aliquot using a Kugelrohr distillation apparatus to give a colourless, crystalline solid upon cooling to RT. The product was analyzed by NMR, HPLC and LC-MS.

3.2 RADIOCHEMISTRY

Fluorine-18 fluoride ($[^{18}F]F^-$) was produced from a GEMS PET trace cyclotron using 16.4 MeV protons via the $^{18}O(p,n)^{18}F$ reaction on ^{18}O enriched water ($[^{18}O]H_2O$). $[^{18}F]F^-$ was isolated from $[^{18}O]H_2O$ on a preconditioned SepPak QMA light anion exchange cartridge and subsequently eluted from the cartridge with a solution of K_2CO_3, Kryptofix-2.2.2 (4,7,13,16,21,24-hexaoxa-1,10-diazabicyclo-[8.8.8]hexaco sane-$K_{2.2.2}$) in water (18 MΩ) and MeCN to a reaction vessel[105]. The solvents were evaporated at 160°C for 10-15 minutes under continuous nitrogen flow to form a dry complex of $[^{18}F]F^-/K^+/K_{2.2.2}$ and the residue was cooled to RT. The chloro or sulphamidate precursors in DMSO were added to the dry complex of $[^{18}F]F^-/K_2CO_3/K_{2.2.2}$. The closed reaction vessel was heated at 120-130°C for 10-20 minutes and cooled down to RT. For deprotection HCl was added to the reaction mixture and heated at 110°C for 10-20 minutes. The reaction mixture was cooled to RT and was diluted with water to a total volume of 2 mL before injecting it into the HPLC for purification. All fluorine-18 labeled radioligands were purified by reverse phase HPLC and MeCN-H_3PO_4 (0.01 M) was used as the eluting solvent. The elute was monitored

by a UV absorbance detector (λ = 214 nm) in series with a GM tube radioactivity detector. The fraction of the desired compounds was either collected, followed by being evaporated to dryness or was diluted with water followed by isolation with SepPak tC18 plus cartridge. The residue was dissolved in sterile phosphate buffered saline (PBS; pH = 7.4; 10 mL) and filtered through a sterile filter (0.22 µm; Millipore, Bedford, MA), yielding a sterile and pyrogen-free (< 1.25 EU/mL) solution of the radioligand.

The radiochemical purity of all radioligands was determined by a reverse phase HPLC on a µ-Bondapak C-18 column (300 X 3.9 mm, 10 µm; waters instruments). The elute was monitored by a UV absorbance detector (λ = 214 nm) in series with a radioactivity detector (β-flow; Beckman, Fullerton, CA). The stability and radiochemical yield was tested with HPLC and TLC on silica gel (100% EtOAc was used as the eluting solvent). TLC plate was scanned with an AR-2000 Imaging Scanner and analyzed with Winscan 2.2 software.

3.3 DETERMINATION OF MAO INHIBITION

Human recombinant MAO-B and MAO-A enzymes prepared from insect cells were purchased from Sigma. The assays were designed to determine the inhibition of kynuramine oxidation in the presence of the compounds of interest according to a previously described methods[116]. The assays were designed to determine the generation of 4-OH-quinoline from kynuramine in the presence of the compounds of interest. A calibration curve of 4-OH quinoline (Sigma) was determined at λ_{Ex}=310 nm/ λ_{Em}=400 nm and used for calculation of the enzyme activity at the respective compound concentration. This relation was plotted and the IC_{50} was determined using the software GraFit 5 (Version 5.0.6). The assays were performed as follows. The compounds were diluted 1:2 in each step in 50 mM PBS (pH 7.4) so that a concentration curve between 0.49 nM and 1000 nM was generated to determine the IC_{50} for MAO-B and between 0.98 and 2000 nM for determination of inhibition of MAO-A, respectively. Kynuramine hydrobromide at a concentration of 125 µM for MAO-B and 100 µM for MAO-A, respectively, and 2.5 U/mL enzyme were added and the reaction followed measuring the absorption at 360 nm in a 5 minutes interval over 30 minutes at 37°C. The 30 minutes time point was used to determine IC_{50} values. As internal standards for MAO-B, pargyline and *L*-deprenyl and for MAO-A clorgyline were used.

3.4 *IN VITRO* AUTORADIOGRAPHY

Human brains without pathology were obtained from the Department of Forensic and Insurance Medicine, Semmelweis University, Budapest and the brains had been removed during forensic autopsy (control brains)[117, 118]. The post mortem time of the human brains was up to 11 hours until which the cadaver was stored at ±0°C. After removal, the brain was kept at -85°C until sectioning and then the whole hemisphere brain slices were kept at -25°C until the autoradiographic procedure began. Ethical

permissions were obtained from the relevant Research Ethics Committee of the respective institution. The sectioning of the brains and the autoradiography experiments were performed at the Department of Clinical Neuroscience, Karolinska Institutet. The sectioning was carried out by a Leica cryomacrocut system, yielding coronal or horizontal slices of 100 µm thickness.

The autoradiographic procedures were identical with those used in previous studies[119]. The whole hemisphere sections were incubated for 90 minutes at RT with 4 MBq/200 mL of the corresponding radioligand in 50 mM TRIS buffer pH 7.4 containing sodium chloride (120 mM), potassium chloride (5 mM), calcium chloride (2 mM) and albumin (0.1 % w/v). After incubation, the sections were washed in the same buffer three times for five minutes each time at RT, briefly dipped in ice cold distilled water, dried and exposed to phosphorimaging plates. The readings were made in a Fujifilm BAS-5000 phosphorimager. Standards were prepared by serial dilution of the radioligand stock solution in assay buffer, using the phosphorimager's Multi Gauge 3.2 image analysis software (Fujifilm). Blocking experiments were performed with 10 µM *L*-deprenyl, rasagiline and pirlindol, respectively.

3.5 PET IN NON-HUMAN PRIMATE

Cynomolgus monkeys (*Macaca Fascicularis*) were supplied by the Astrid Fagraeus Laboratory of the Swedish Institute for Infectious Disease Control (SMI), Solna, Sweden. The study was approved by the Animal Ethics Committee of the Swedish Animal Welfare Agency and was performed according to "Guidelines for planning, conducting and documenting experimental research" (Dnr 4820/06-600) of the KI as well as the "Guide for the Care and Use of Laboratory Animals"[120]. Anesthesia was induced by repeated intramuscular injections of a mixture of ketamine hydrochloride (3.75 mg/kg/h Ketalar® Pfizer) and xylazine hydrochloride (1.5 mg/kg/h Rompun® Vet., Bayer). The head of the monkey was fixed during the PET experiments[121]. Body temperature was maintained by Bair Hugger-Model 505 (Arizant Health Care Inc., MN, USA) and monitored by an oral thermometer. ECG, heart rate, respiratory rate and oxygen saturation were continuously monitored throughout the experiments and blood pressure was monitored every 15 minutes.

The PET measurement was performed using a High Resolution Research Tomograph (HRRT) (Siemens Molecular Imaging) PET scanner[122]. List-mode data were reconstructed using the ordinary Poisson-3D-ordered subset expectation maximization (OP-3D-OSEM) algorithm, with 10 iterations and 16 subsets including modeling of the point spread function (PSF). A transmission scan of 6 minutes using a single ^{137}Cs source was performed immediately before the injection of the radioligand. List-mode data were acquired continuously for 120 minutes at the same time as the intravenous injection of the radioligand. During reconstruction the list mode data was subdivided into the following series of frames: 9x20 sec, 3x60 sec, 5x180 sec, 17x360 sec.

Brain MRI was performed in a 1.5-T GE Signa system (General Electric, Milwaukee, WI, USA). A T1 weighted image was obtained for coregistration with PET and the delineation of anatomic brain regions. The T1 sequence was a 3D spoiled gradient recalled (SPGR) protocol with the following settings: repetition time (TR) 21 ms, flip angle 35˚; FOV 12.8; matrix 256x256x128; 128x1.0 mm slices; 2 NEX. The sequence was optimized for a trade-off between a minimum of scanning time and a maximum of spatial resolution and contrast between gray and white matter.

Before delineation of regions of interests (ROIs), the orientation of the brain was spatially normalized by having the high-resolution T1-weighted magnetic resonance images reoriented according to the line defined by the anterior and posterior commissures being parallel to the horizontal plane and the inter-hemispheric plane being parallel to the sagittal plane. The T1-weigted MR images were then re-sliced to the resolution of the HRRT PET system, 1.219x1.219x1.219 mm. The standardized T1-weighted MR images were used as an individual anatomical template for the monkey.

Regions of interest (ROIs) (the whole brain, the striatum, thalamus, cortex and cerebellum) were delineated on the realigned MRI image with the reference to the co-registered PET using PMOD 3.1 (Zurich, Switzerland). Measurement of the uptake were analyzed by using standardized uptake value (SUV), which is the regional tissue radioactivity concentration normalized for the injected dose and body weight of the monkey.

$$\%\text{SUV} = \frac{\%\ \text{injected activity}}{\text{brain tissue (ccm)}}\text{body weight (g)}$$

3.6 RADIOMETABOLITE ANALYSIS

Radiometabolite analysis was done by following a modified method used for other radioligands[41]. A reverse phase gradient radio-HPLC method was used for determination of the percentages of radioactivity corresponding to unchanged radioligands and radiometabolites during the course of a PET measurement. Venous blood samples (2 mL) were obtained from the monkey at different time points such as 4, 15, 30, 45, 60, and 75 minutes after the injection of the radioligands. Plasma samples (0.5 mL) obtained after the centrifugation of blood at 2000 *g* for 2 minutes was mixed with acetonitrile (0.7 mL). The supernatant acetonitrile-plasma mixture (1.1 mL) was injected to a HPLC and the precipitate obtained after centrifugation at 2000 g for 2 minutes was counted in a NaI well-counter. The well-counter consists of a NaI crystal (Harshaw, diameter: 38 mm x 50 mm; diameter of the well: 16 mm; depth: 38 mm). The crystal was housed inside a led shield cylinder with a wall thickness of approx 5 cm. Furthermore, the crystal was coupled to a high voltage supply, set to 900V (Canberra, model 3002), an energy discriminator (Canberra, model 818) and a timer and counter (GE&E Ortec, model 871). Radioactive peaks eluting from the column were integrated and their areas expressed as a percentage of the sum of the areas of all

the detected radioactive peaks (decay-corrected). To calculate the recovery of radioactivity from the system, an aliquot (2 mL) of the eluate from the HPLC column was measured and divided with the amount of total injected radioanalyte.

4 RESULT AND DISCUSSIONS

4.1 SYNTHESIS, RADIOLABELING AND BIOLOGICAL EVALUATION OF FLUORO ANALOGUES OF *L*-DEPRENYL FOR MAO-B (PAPER I AND PAPER II)

Selegiline or *L*-deprenyl was the first compound discovered as a selective irreversible MAO-B inhibitor[67]. The action of *L*-deprenyl in the human brain is two-fold. Firstly, it preserves dopamine by selective inhibition of MAO-B and secondly, it inhibits the re-uptake of dopamine and increases the synthesis rate of dopamine[123-125]. *L*-Deprenyl itself has been labeled with carbon-11 and was demonstrated as useful tracer for assessing MAO-B[80, 81, 126]. In this study we labeled *L*-deprenyl analogues with fluorine-18 at different positions and evaluated their biological activity as PET radioligands for imaging brain MAO-B.

4.1.1 Chemistry and radiochemistry

Three novel fluorinated analogues of *L*-deprenyl *N*-(2-fluoroethyl)-*N*-(1-phenylpropan-2-yl)prop-2-yn-1-amine (**2**), *N*-((1*R*,2*S*)-1-fluoro-1-phenylpropan-2-yl)-*N*-methylprop-2-yn-1-amine (**8**) and (*S*)-*N*-(1-fluoro-3-phenylpropan-2-yl)-*N*-methyl prop-2-yn-1-amine (**13**) were synthesized by multistep organic synthesis according to scheme 2. Three appropriate chloro-precursors *N*-(2-chloroethyl)-*N*-(1-phenylpropan-2-yl)prop-2-yn-1-amine (**4**), *N*-((1*R*,2*S*)-1-chloro-1-phenylpropan-2-yl)-*N*-methylprop-2-yn-1-amine **(9)** and a isomeric mixture of (*S*)-*N*-(1-chloro-3-phenylpropan-2-yl)-*N*-methylprop-2-yn-1-amine (**14)** and *N*-(2-chloro-3-phenylpropyl)-*N*-methylprop-2-yn-1-amine (**15)** for labeling with fluorine-18 were also synthesized. The formation of the isomeric mixtures of chlorides **14** and **15** can be explained by an intermediate aziridinium ion **17** resulting from an intramolecular nucleophilic attack (S_Ni) of the free electron pair of nitrogen[127] according to scheme 3. Chlorides **14** and **15** were then formed by the subsequent nucleophilic attack (S_N2) of Cl^- at the corresponding reactive position of aziridinium ion **17**. All compounds were identified by HPLC, NMR and LC-MS.

The radiolabeling of all three compounds *N*-[2-[^{18}F]fluoroethyl]-*N*-[(2R)-1-phenylpropan-2-yl]prop-2-yn-1-amine (**4a**), *N*-[(1S,2R)-1-[^{18}F]fluoro-1-phenyl propan-2-yl]-*N*-methylprop-2-yn-1-amine (**4b**) and *N*-[(2S)-1-[^{18}F]fluoro-3-phenyl propan-2-yl]-*N*-methylprop-2-yn-1-amine ([^{18}F]fluorodeprenyl, **4c**) was achieved by a one-step nucleophilic substitution reaction according to scheme 2. Compound **4c** was purified from the isomeric mixture by reversed phase HPLC. The overall radiosynthesis including radiofluorination, HPLC purification, and evaporation of the solvent and radiotracer formulation was completed in a time range of 70-80 minutes. The incorporation yield of the fluorination reactions varied from 40% to 70%, the radiochemical purity was greater than 99% and SA varied from 200 to 270 GBq/µmol

for all three radioligands. The identities of the labeled compounds were confirmed by co-injection of their corresponding fluorine-19 analogues **2**, **8** and **13** using analytical HPLC. All three radioligands were found to be stable in PBS buffered solution (pH=7.4) for the duration of 120 min.

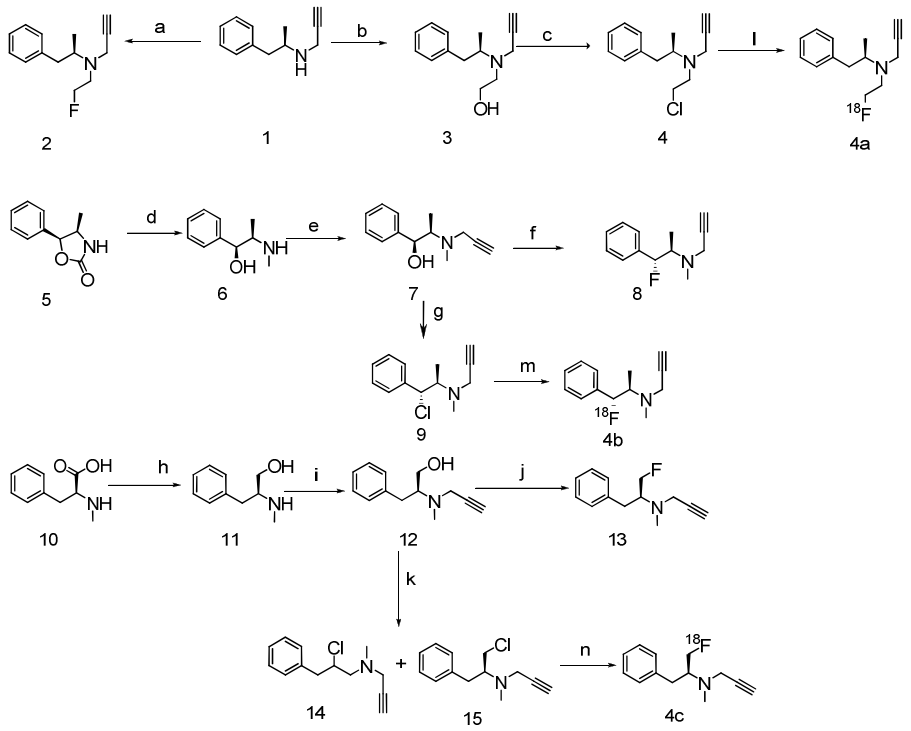

Scheme 2: Synthesis of precursors, reference standards and radiolabeling.
Conditions: a: NaOH/1-fluoro 2-bromo ethane;b: NaOH/1-bromo ethanol; c: TEA/mesyl chloride; d: LAH; e: K_2CO_3/propargyl bromide; f: DAST; g: TEA/mesyl chloride; h: LAH; i: K_2CO_3/propargyl bromide; j: DAST; k: TEA mesyl chloride; l,m,n: $K^{18}F$, K-2,2,2/DMSO.

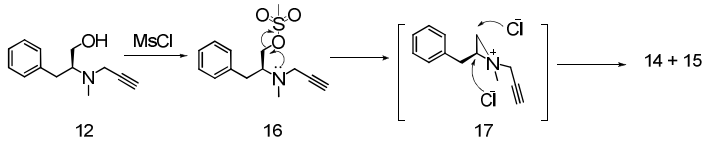

Scheme 3: Proposed mechanism for the formation of **14** and **15**.

4.1.2 *In vitro* inhibition and autoradiography

Compounds **2** and **8** inhibited MAO-B with an IC_{50} greater than 2 µM and were therefore, not further investigated. Compound **13** featured an IC_{50} of 31 ± 2.2nM for its MAO-B inhibitory activity while it was not inhibiting MAO-A (IC_{50}>50 µM). *L*-Deprenyl was used as a reference compound. It inhibited MAO-B with an IC_{50} of 13±0.4 nM. Thus, compound **13** inhibited MAO-B in a range comparable to that of the therapeutically used compound.

Compound **4c** was demonstrated as a selective radioligand for the MAO-B enzyme by human brain ARG (Figure 3). At baseline condition (panel A) it shows binding to brain regions known to have a high content of MAO-B. For blocking, the MAO-B ligands *L*-deprenyl (panel B), rasagiline (panel C) and the MAO-A ligand pirlindole (panel D) were used. Using the MAO-B ligands rasagiline and *L*-deprenyl the binding of **4c** was completely blocked, whereas the MAO-A ligand pirlindole did not significantly block the total binding. This indicates that **4c** is a selective radioligand of the MAO-B enzyme.

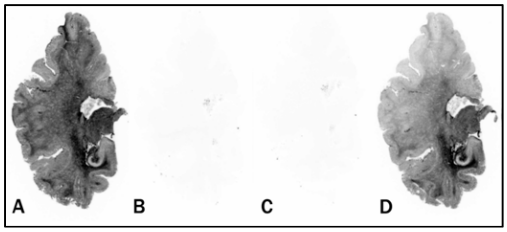

Figure 3. Coronal slices of human brain autoradiograms labeled with **4c**. (A) Baseline conditions. (B) Incubation with *L*-deprenyl (10 µM), (C) Incubation with rasagiline (10 µM), (D) Incubation with pirlindole (10 µM).

4.1.3 Biodistribution in mice and PET in non-human primate

The biodistribution of compound **4c** in mice showed a high initial brain uptake of radioactivity levelling at 5.2 ± 0.04 %ID/g at two minutes post injection (p.i.). The initial elimination of radioactivity from the brain was observed reaching a level of 1.9 ± 0.33 % ID/g at 30 minutes (Figure 4). The biodistribution of compound **4c** decreases as a function of time which differs to the literature data for [^{11}C]deprenyl brain kinetics in mice[80] where it increases as a function of time. It could be explained by that **4c** is a chemically different compound as compared to deprenyl itself and/or the differences of the mouse strain, used in the experiment.

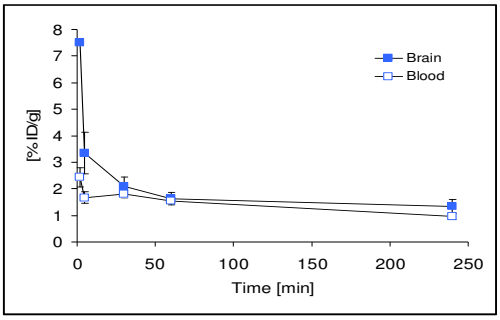

Figure 4: Time course distribution of compound **4c** in brain and blood of male NMRI mice.

In comparative PET measurements, **4c** in a cynomolgus monkey indicated irreversible binding kinetics similar to the binding characteristics obtained by [^{11}C]deprenyl[81] and the uptake of [^{18}F]fluorodeprenyl at baseline condition was highest in the striatum followed by the thalamus, the cortex and the cerebellum (Figure 5 and 6).

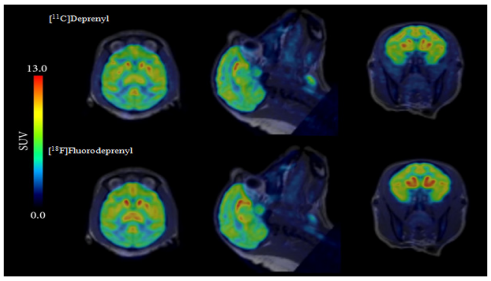

Figure 5. PET images of [^{11}C]deprenyl and [^{18}F]fluorodeprenyl (**4c**) co-registered with MRI averaged between 9 and 120 min in the horizontal (left), sagittal (middle) and coronal (right) projections (left)

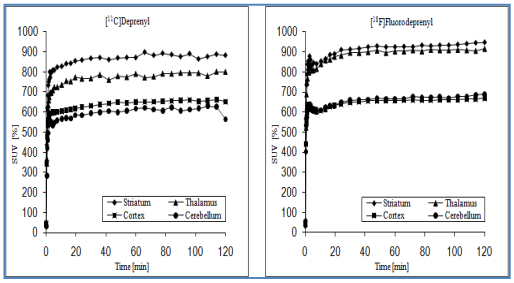

Figure 6. Brain uptake expressed as percent standardised uptake value (%SUV) in different brain regions after i.v. injection of [^{11}C]deprenyl (left) and [^{18}F]fluorodeprenyl (**4c**) (right)

Pre-administration of *L*-deprenyl (5 mg/kg) to the monkey resulted in about a six to eight fold decrease of radioactive uptake of **4c** in the investigated brain regions (Figure 7 and 8). This effect was similar to that reported for [^{11}C]deprenyl in the baboon brain[128].

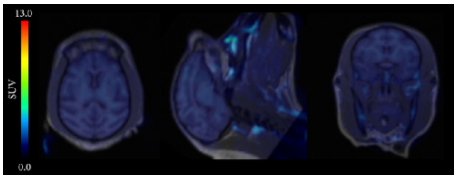

Figure 7. PET images of **4c** co-registered with MRI averaged between 9 and 120 minutes in the horizontal (left), sagittal (middle) and coronal (right) projections after pretreatment with L-deprenyl (5 mg/kg)

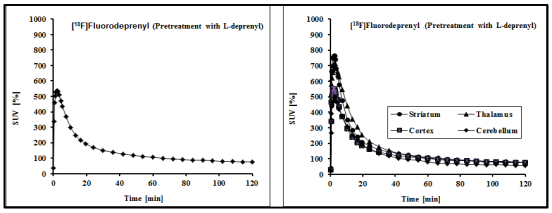

Figure 8. Brain uptake expressed as percent standardised uptake value (%SUV) after pretreatment with *L*-deprenyl (5 mg/kg). Time activity curves after i.v. injection of **4c** in whole brain (left) and in different brain regions (right)

4.1.4 Radiometabolites measured in plasma

Compound **4c** showed relatively slower metabolism measured in monkey plasma compared to [^{11}C]deprenyl. At 15 minutes p.i., approximately 38% of the plasma radioactivity was unchanged [^{11}C]deprenyl, decreasing to 16% at 45 minutes p.i. whereas at 15 minutes after injection of **4c** approximately 58% of the plasma radioactivity was unchanged parent radioligand, decreasing to 32% at 45 and 22% at 120 minutes p.i. (Figure 9).

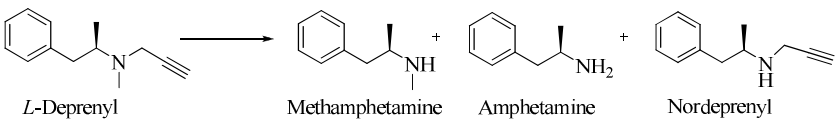

Scheme 4: Proposed metabolism of *L*-deprenyl[129].

Radiometabolites of [^{11}C]deprenyl have been extensively studied previously and found mainly to correspond to [^{11}C]formic acid and its adducts, as well as [^{11}C]methamphetamine[129-132]. It is also reported that three major urinary metabolites of *L*-deprenyl hydrochloride (*N*-methyl-*N*-propargyl(2-phenyl-1-methyl)ethylammonium chloride), were identified after administration to humans (Scheme 4). Compound **4c** showed a similar pattern of metabolism measured in monkey plasma reported for [^{11}C]deprenyl. Therefore, there is a possibility of radiometabolites crossing the BBB and may complicate the quantification of PET data.

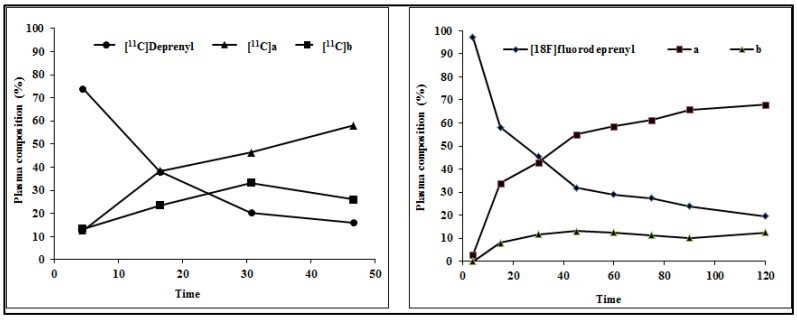

Figure 9. Radiometabolite analysis during the time course of the PET measurements, [^{11}C]deprenyl (left) and [^{18}F]fluorodeprenyl (**4c**) (right).

4.2 SYNTHESIS, RADIOLABELING AND BIOLOGICAL EVALUATION OF [^{18}F]FLUORORASAGILINE FOR MAO-B (PAPER III)

Rasagiline is a selective and irreversible MAO-B inhibitor which is co-administrated for the treatment of relieving symptoms resulting from the loss of dopaminergic neurons in Parkinson's disease[133]. The two main metabolites of rasagiline are aminoindane and hydroxyaminoindan (Scheme 5) which in contrast to the amphetamine-like metabolites of *L*-deprenyl does not increase noradrenaline potency nor does it display any MAO-B inhibitory activity[134, 135]. Therefore, we used fluorinated rasagiline as the chemical entity for the development of a novel MAO-B PET ligand.

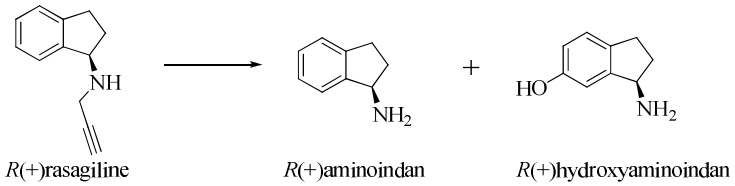

Scheme 5: Proposed metabolism of *R*-rasagiline[135].

4.2.1 Chemistry and radiochemistry

The precursor (3a*S*,8a*R*)-3-[prop-2-yn-1-yl]-3,3a,8,8a-tetrahydroindeno- [1,2-d][1,2,3] oxathiazole 2,2-dioxide (**20**) was synthesized from the starting material aminoindanol

(**18**) by multistep organic synthesis following a previously reported method[136] (Scheme 6). In the first step, **18** was treated with highly reactive sulfuryl chloride and the key parameter of this reaction was to keep the temperature at -65°C. In the second step, tetrahydroindeno[1,2-d][1,2,3]oxathiazole 2,2-dioxide (**19**) was alkylated with propargyl bromide to give the precursor compound (**3**) in a moderate 68% isolated yield, following a previously reported method[136].

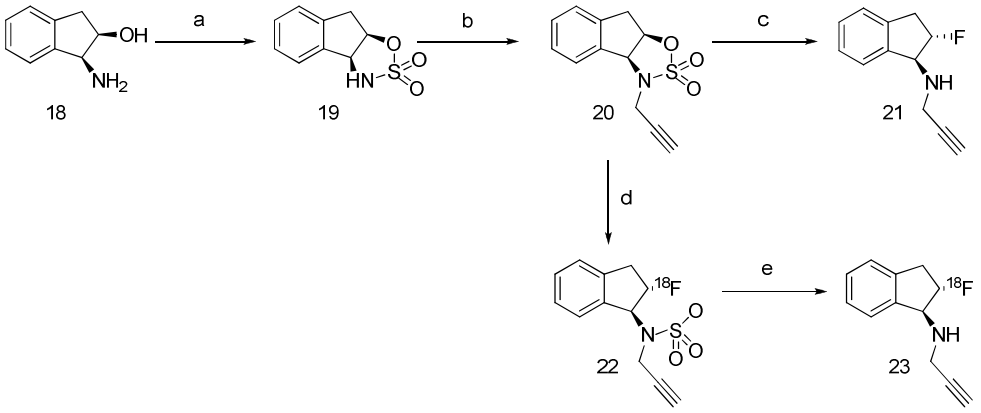

Scheme 6. Synthesis of precursor (**20**) and reference standard (**21**) and [^{18}F]fluororasagiline (**23**).
Conditions: a: SO_2Cl_2/triethylamine; b: K_2CO_3/ propargyl bromide; c: CsF/5N HCl; d: K^{18}F, K-2,2,2/DMSO e: 0.5N HCl.

The reference standard (1*S*,2*S*)-2-fluoro-*N*-(prop-2-yn-1-yl)-indan-1-amine (fluororasagiline, **21**) was synthesized by two step synthesis from **20**. The first step was substitution reaction with cesium fluoride followed by the hydrolysis of the sulphamidate group (Scheme 6). All compounds were identified by HPLC, NMR and LC-MS.

The radiolabeling of (1*S*,2*S*)-2-[^{18}F]fluoro-*N*-(prop-2-yn-1-yl)-indan-1-amine ([^{18}F]fluororasagiline, **23**) was achieved by nucleophilic substitution of the sulphamidate precursors (**20**) by [^{18}F]fluoride followed by deprotection of the sulphamidate group (Scheme 6). Different acids such as sulfuric acid, trifluoroacetic acid, hydroiodic acid and hydrochloric acid were tested for the hydrolysis of the sulphamidate group and 200 µL of 0.5N hydrochloric acid gave the highest yield. The radiochemical yield of the radiosynthesis was 50-55%, the radiochemical purity was higher than 99% and SA varied from 240 to 265 GBq/µmol for the radioligand. The identity of the labeled compound was confirmed by the co-injection of its corresponding fluorine-19 analogue **21** using analytical HPLC. Compound **23** was found to be stable in PBS buffered solution (pH=7.4) for the duration of 120 minutes.

4.2.2 *In vitro* inhibition and autoradiography

Inhibition of the enzymatic activities of MAO-B and MAO-A by fluorine-19 analogue of rasagiline (**21**) was determined based on the rate of 4-OH-quinoline generation from

kynuramine. The compound inhibited MAO-B with an IC_{50} = 27.0 ± 2.0 nM compared to rasgiline itself IC_{50} = 46.0 ± 2.2 nM. It is inhibiting MAO-A with an IC_{50} = 2.3 ± 0.08 µM. Compound **21** was ca. 84 times more potent in inhibiting MAO-B versus MAO-A hinting at its specificity.

Human whole hemisphere ARG was performed with **23**. The signal intensities were highest in the hippocampus, the putamen, the caudate nucleus, the external globus pallidus and the thalamus. For blocking, the MAO-A ligand pirlindole and the MAO-B ligands *L*-deprenyl and rasagiline have been used in 10 µM concentrations (Figure 10). The MAO-B ligands rasagiline and *L*-deprenyl completely blocked the binding of **23**, whereas the MAO-A ligand pirlindole did not block the binding. These observations indicate that **23** is a selective radioligand of MAO-B, whereas it displays negligible binding to the MAO-A isoform.

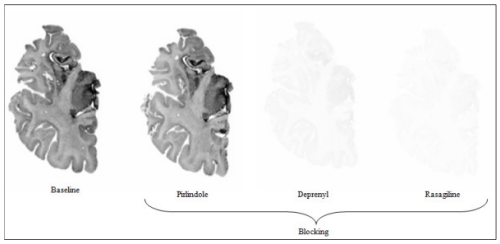

Figure 10. Coronal slices of human brain autoradiograms labeled with **23** at baseline condition and incubation with pirlindole (10 µM), *L*-deprenyl (10 µM) and rasagiline (10 µM).

4.2.3 PET in non-human primate

Following the injection of **23** in a cynomolgus monkey, a reasonable amount (250 % SUV at 4 minutes p.i.) of radioactivity entered the brain (Figure 11 and 12). Due to the irreversible binding kinetics, [^{18}F]fluororasagiline did not show any wash-out from the brain and the uptake of radioactivity at baseline condition was highest in the striatum and thalamus and lowest in the cerebellum and in cortical areas.

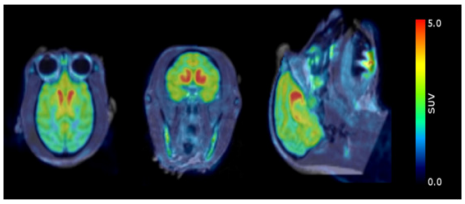

Figure 11. PET images of **23** co-registered with MRI and averaged between 9 and 120 minutes in the horizontal (left), coronal (middle) and sagittal (right) projections.

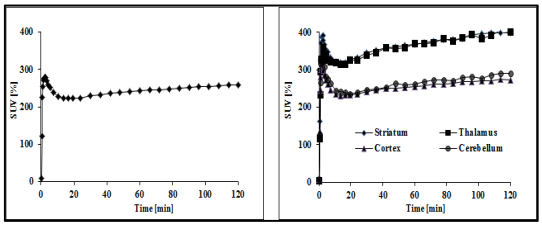

Figure 12. Brain uptake expressed as percent standardised uptake value (%SUV) after i.v. injection of **23**, in whole brain (left) and time activity curves in different brain regions (right).

4.2.4 Radiometabolites measured in plasma

The metabolism of **23** was moderate and at 30 minutes approximately 60% of the plasma radioactivity represented the parent compound (Figure 13 (right)). HPLC

analysis of the plasma following the injection of **23**, which eluted at 7.7 minutes, revealed the presence of three more major peaks, [^{18}F]a**,** [^{18}F]fluoroaminoindan and [^{18}F]b with retention times of 2.7, 4.6 and 9.2 minutes, respectively (Figure 13 (left)).

Despite the promising brain uptake, the experiment revealed one potential problem with **23**, namely that the radioactivity continued to increase slowly throughout the PET measurement. This finding may be explained by the brain penetration of radiometabolites.

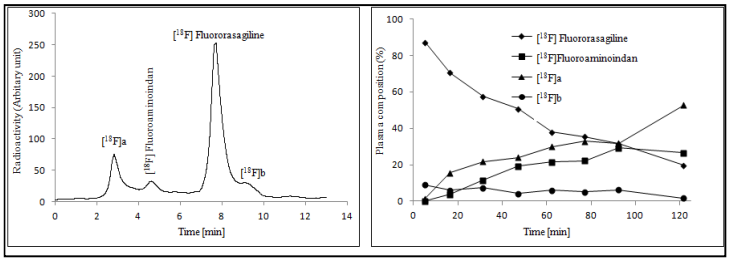

Figure 13 . Radiometabolite analysis at 30 minutes p.i. of [^{18}F]fluororasagiline (**23**) (left) and during the time course of the PET measurements (right).

4.3 SYNTHESIS, RADIOLABELING AND BIOLOGICAL EVALUATION OF ONE HETEROAROMATIC AND TWO ALIPHATIC PROPARGYL AMINES FOR MAO-B (PAPER IV)

MAO-B can be irreversibly inactivated by propargylamine derivatives, where the oxidized propargylamine derivative binds to the flavin group of corresponding highly electrophilic eyiminium species by a covalent bond forming an adduct leading to inactivation of the enzyme by micromolar concentrations[60]. In this study we designed one heteroaromatic propargylamine derivative ((*S*)-*N*-(1-fluoro-3-(furan-2-yl)propan-2-yl)-*N*-methylprop-2-yn-1-amine (**33**)) and two aliphatic propargylamine derivatives ((*S*)-1-fluoro-*N*,4-dimethyl-*N*-(prop-2-ynyl)pent-4-en-2-amine (**28**) and (*S*)-1-fluoro-*N*,4-dimethyl-*N*-(prop-2-ynyl)pentan-2-amine (**38**)). Our aims were to prepare the precursors and reference standards and to develop efficient synthetic methods for labeling these radioligands with fluorine-18 and to evaluate their biological properties as PET radioligands for imaging MAO-B in the brain.

4.3.1 Chemistry and radiochemistry

Three novel fluorinated derivatives of propargyl amine **28**, **33** and **38** (Scheme 7) were synthesized. In order to obtain respective radioligands three appropriate chloro-precursors were also synthezised by multi-step organic synthesis. Amines **25**, **30** and **35** were prepared from the commercially available amino acid (*S*)-2-(*tert*-butoxycarbonylamino)-4-methylpent-4-enoic acid (**24**), (*S*)-*tert*-butyl 1-(furan-2-yl)-3-hydroxypropan-2-ylcarbamate (**29**) and the amino acid (*S*)-4-methyl-2-(methylamino)-pentanoic acid (**34**) by reduction with $LiAlH_4$ following a previously described

procedure.[137] Amino alcohols **24**, **29** and **34** were alkylated with propargyl bromide[136] and the obtained respective alcohols **26**, **31** and **33** were chlorinated by treatment with mesyl chloride to synthesize the chloro precursors respectively. The formation of a mixture of two chlorinated isomers can be explained by a corresponding intermediate aziridinium ion resulting from an intramolecular nucleophilic attack (S_Ni) of the free electron pair of the nitrogen.[127] Reference standards **28** and **33** were synthesized from amino alcohols **26** and **31** by fluorination reaction with diethylamino sulfurtrifluoride (DAST) and reference standard **38** was synthesized from amino alcohol **36** by treating with triethylamine trihydrofluoride. All compounds were identified by HPLC, NMR and LC-MS.

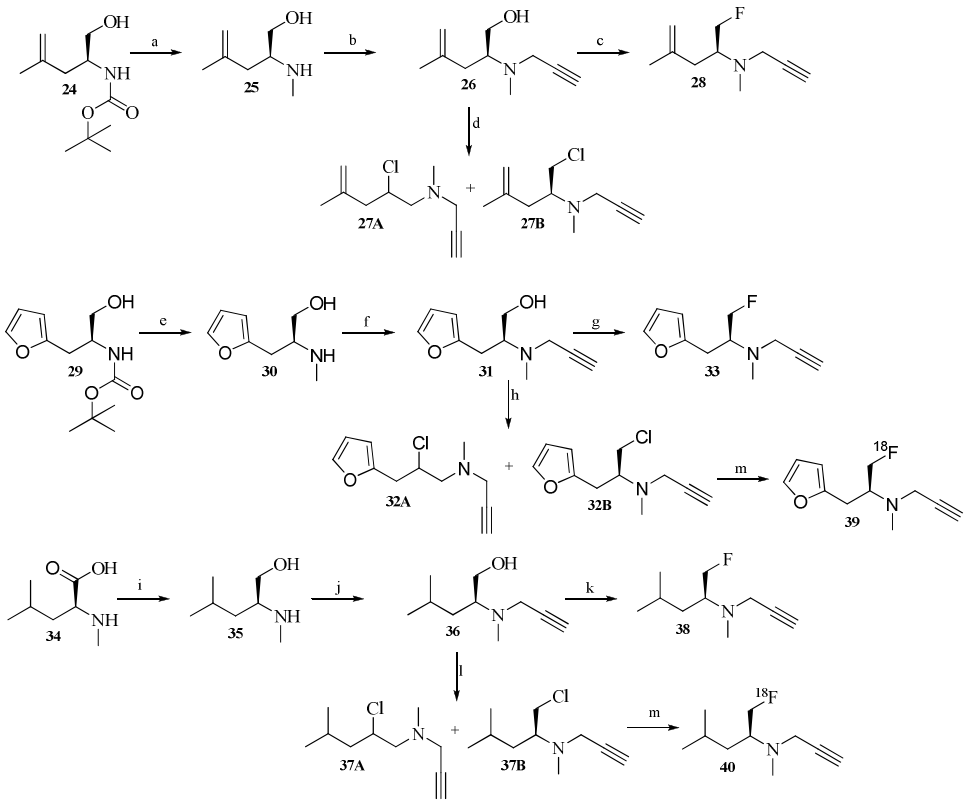

Scheme 7. Synthesis of precursors and reference standards and radiolabeling of **39** and **40**.
Conditions: a: LAH; b: K_2CO_3/ propargyl bromide; c: DAST; d: pyridine/ mesyl chloride; e: LAH; f: K_2CO_3/ propargyl bromide; g:DAST; h: TEA/ mesyl chloride; i: LAH; j: K_2CO_3/ propargyl bromide; k: TEA/ DAST; l: TEA/ mesyl chloride; m: $K^{18}F$, K-2,2,2/DMSO/ K_2CO_3.

The radiolabeling of (*S*)-*N*-(1-[^{18}F]fluoro-3-(furan-2-yl)propan-2-yl)-*N*-methylprop-2-yn-1-amine (**39**) and (*S*)-1-[^{18}F]fluoro-*N*,4-dimethyl-*N*-(prop-2-ynyl)pentan-2-amine (**40**) was achieved by one step nucleophilic substitution reactions of the corresponding chloride precursors by [^{18}F]fluoride in presence of $K_{2.2.2}$ and K_2CO_3 as shown in scheme 7. Compounds **39** and **40** were purified from the corresponding reaction mixtures by semi preparative HPLC. The overall radiosynthesis including fluorination, HPLC purification, and evaporation of the solvent and radiotracer formulation was completed in a time range of 70-80 minutes. The incorporation yield of the fluorination reactions from fluorine-18 ion varied from 40% to 60%, and the radiochemical purity

was greater than 99% for both radiosynthesis. The specific radioactivity for **40** was between 192 and 240 GBq/µmol. The identities of the labeled compounds were confirmed by co-injection of their corresponding fluorine-19 analogues **33** and **38** using analytical HPLC. Both radioligands were found to be stable in PBS buffered solution (pH=7.4) for the duration of 150 minutes.

4.3.2 *In vitro* inhibition and autoradiography

IC_{50} values for inhibition were determined for compounds **28**, **33** and **38** in order to determine their specificity for binding to MAO-B. Compound **28** inhibited MAO-B with an IC_{50} of 664 ± 48.08 nM and was discarded without further investigation. Whereas compounds **33** and **38** inhibited MAO-B in a range comparable to that of the therapeutically used compound deprenyl with IC_{50} values of 208.5 ± 13.44 nM and 131.5 ± 0.71 nM. Therefore **33** and **38** were chosen for labeling with fluorine-18 for further investigation by ARG.

The ARG signal intensities for both **39** and **40** were highest in the hippocampus, the putamen, the caudate nucleus and the thalamus. In order to test the specificity of the compound the binding was blocked with an excess (10 µM) of the MAO-B ligands *L*-deprenyl and rasagiline and of the MAO-A ligand pirlindole, respectively (Figure 14). The MAO-B ligands rasagiline and *L*-deprenyl completely blocked the total binding of both **39** and **40.** The MAO-A ligand pirlindole did not block the total binding **40** whereas it could partly block the total binding of **39**. These observations indicated that compound **40** is a selective radioligand of the MAO-B enzyme. Consequently, **40** was chosen for further examination using PET measurements of its brain uptake and distribution in a cynomolgus monkey.

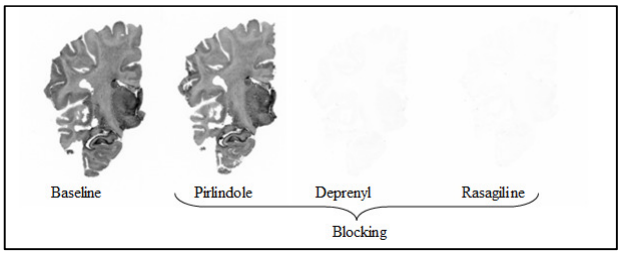

Figure 14. Coronal slices of human brain autoradiograms labeled with **40** at baseline condition and incubation with pirlindole (10 µM), *L*-deprenyl (10 µM) and rasagiline (10 µM).

4.3.3 PET in non-human primate

At baseline condition compound **40** readily crossed the BBB and bound rapidly to its target sites with a high brain uptake (250% SUV at 4 minutes) (Figure 15 and 16) but it was considerably lower than [^{18}F]fluorodeprenyl (**4c**) (600-900% SUV at 4 minutes). Due to the irreversible binding kinetics, compound **40** did not show any wash-out from the brain. The uptake was highest in the striatum and the thalamus and lower in the cerebellum and the cortical areas, consistent with the known distribution of MAO-B

activity as previously reported for [^{11}C]deprenyl[81], and similar to what we found ourselves for **4c** and **23** in this work.

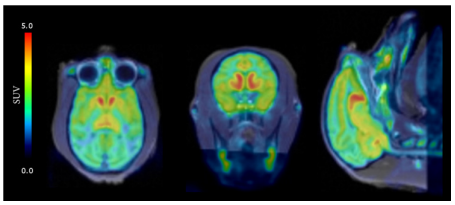

Figure 15. PET images of **40** co-registered with MRI and averaged between 9 and 120 minutes in the horizontal (left), coronal (middle) and sagittal (right) projections.

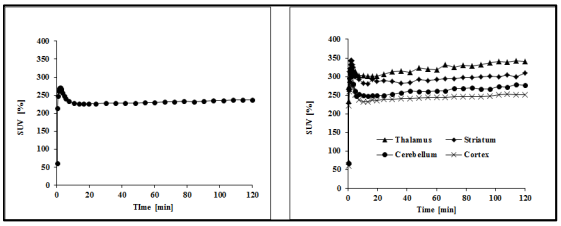

Figure 16. Brain uptake expressed as percent standardised uptake value (%SUV) after i.v. injection of **40**, in whole brain (left) and time activity curves in different brain regions (right).

4.3.4 Radiometabolites measured in plasma

The metabolic stability of **40** was lower compared to [^{18}F]fluorodeprenyl and [^{18}F]fluororasagiline and at 45 minutes only approximately 20% of the plasma radioactivity represented the parent compound and it decreased to 12% at 120 minutes (Figure 15). HPLC analysis of plasma following the injection of **40**, which eluted at 7.3 minutes, revealed the presence of five more major peaks with retention times of 2.0, 3.4, 3.7, 4.2 and 6.2 minutes, respectively (Figure 17).

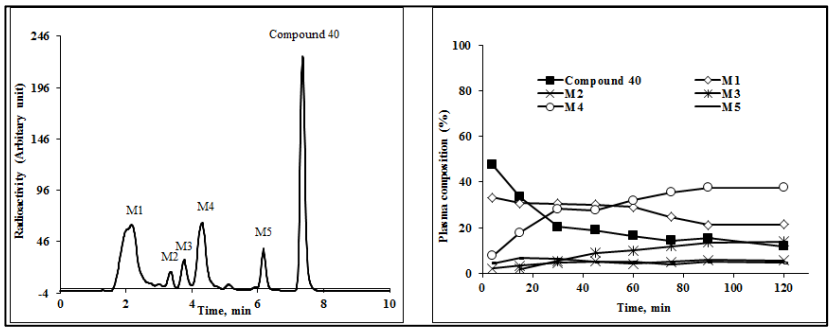

Figure 17 . Radiometabolite analysis at 15 minutes p.i. of **40** (left) and during the time course of the PET measurements (right).

Despite the promising brain uptake and distribution, the experiment revealed one potential problem that the radioactivity continued increasing slowly throughout the PET measurement. This finding may be explained by the brain penetration of radiometabolite(s).

4.4 SYNTHESIS, RADIOLABELING AND BIOLOGICAL EVALUATION OF [^{18}F]FLUORODEPRENYL-D_2 AND [^{18}F]FLUORORASAGILINE-D_2 FOR MAO-B (PAPER V AND PAPER VI)

Kinetic isotope effect has widely been used in the elucidation of organic as well as in enzymatic reaction mechanism[138]. The deuterium isotope effect plays an important role

in the oxidative deamination of amines by MAO[139]. Thus the MAO-B catalyzed bond cleavage of a carbon-hydrogen bond of propargyl group at the α carbon is the rate limiting step in the retention of radioligand in the brain[140]. Therefore, in the rate-limiting step of the enzymatic catalysis, MAO-B cleaves a C–D bond in the methylene group of the propargyl group and generates a reactive intermediate that irreversibly binds to the enzyme[141]. The energy required to cleave the C-D bond is higher than that required to cleave the C-H bond and the substitution of hydrogen atoms with deuterium atoms, reduces the rate of cleavage[142].

Applying this principle earlier, the deuterium substituted analogue of [^{11}C]deprenyl ([^{11}C]deprenyl-D_2) was developed to image MAO-B in brain demonstrating lower uptake and better sensitivity compared to [^{11}C]deprenyl[83, 84, 143, 144]. This study is the continuation of our previous study (paper II and paper III) where we reported *in vivo* evaluation of MAO-B in cynomolgus monkey brain using **4c** and **23**. In order to reduce the rate of radioligand trapping in human brain and thus, to improve its sensitivity as well as in order to reduce the amount of radiometabolites in blood plasma which potentially can penetrate the BBB and thereby may complicate reliable quantification, both **4c** and **23** were deuterated.

4.4.1 Chemistry and radiochemistry

Precursors (**46** and **48**) and reference standards (**45** and **49**) were synthesized in multi-step organic syntheses from the starting material propiolic acid (Scheme 8). The intermidate (1,1-$^2H_2$)prop-2-yn-1-ol (**42**) was synthesized by treating propiolic acid with lithium aluminum deuteride. The key parameter of this reaction was to keep the temperature at below 50°C and purification of the compound because of its low boiling point. In the second step, **42** was brominated with PBr_3 to synthesise the compound (1,1-$^2H_2$)3-bromoprop-1-yne (**43**). Compound **44** was synthesized from **43** and the previously synthesized compound (4*R*,5*R*)-4-methyl 5-phenyl-3-(prop-2-ynyl) oxazolidin-2-one following a previously described procedure[136]. The formation of regioisomeric chlorides **46a** and **46b** can be explained by an intermediate aziridinium ion resulting from an intramolecular nucleophilic substitution attack (S_Ni) of the free electron pair of the nitrogen which has been previously described elsewhere [127]. Compound **48** was synthesized from **43** and the the previously synthesized compound tetrahydroindeno[1,2-d][1,2,3]oxathiazole 2,2-dioxide following a previously reported method. Reference standard (1*S*,2*S*)-2-fluoro-*N*-[(1,1-$^2H_2$)prop-2-yn-1-yl]indan-1-amine (**49**) was synthesized with an inversion of configuration from **48** by a two-step synthesis. The first step was a substitution reaction with cesium fluoride where the cyclic sulphamidate group was opened by a fluoride ion followed by the hydrolysis of the sulphamidate group by addition of 4N hydrochloric acid and ethanol. All compounds were identified by NMR, HPLC and LC-MS.

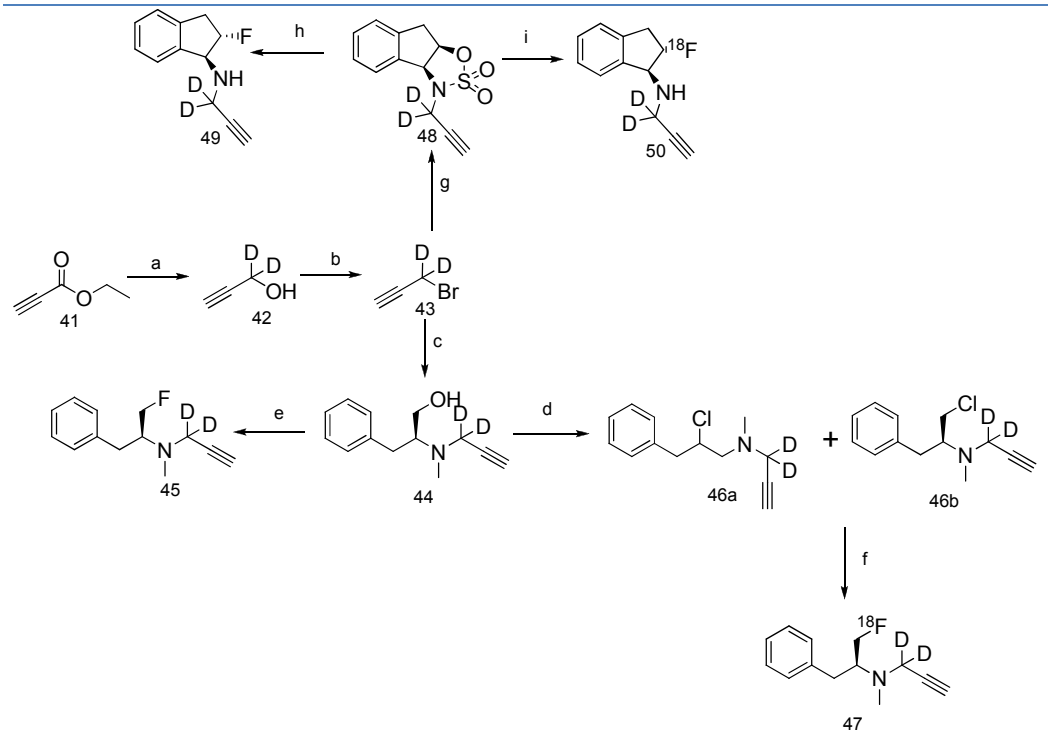

Scheme 8. Synthesis of precursors and reference standards and radiolabeling of [^{18}F]fluorodeprenyl-D_2 (**47**) and [^{18}F]fluororasagiline-D_2 (**50**).
Conditions: a: LAD; b: PBr_3; c: K_2CO_3/ *S*)-2-(methyl(prop-2-ynyl)amino)-3-phenylpropan-1-ol; d: pyridine/mesyl chloride; e: DAST; f: K^{18}F, K-2,2,2/DMSO/ K_2CO_3; g: (3a*S*,8a*R*)-3,3a,8,8a-tetrahydro indeno[1,2-*d*][1,2,3]oxathiazole 2,2-dioxide/ K_2CO_3; h: CsF/5N HCl; i: K^{18}F, K-2,2,2/DMSO/ K_2CO_3

Radiolabeling of both compounds was accomplished by a nucleophilic substitution reaction via S_N2 mechanism and the deprotection of sulphamidate group in the case of **50**, hydrolysis was performed with 150 µL of 1.0 N hydrochloric acid. The incorporation radiochemical yield from fluorine-18 ion was 35-50%. The radiochemical purity was higher than 99% and the specific radioactivity was in a range of 200 to 235 GBq/µmol at the time of administration for both **47** and **50**. Both radioligands were found to be stable at three hours after formulation in a sterile phosphate buffered solution (pH = 7,4).

4.4.2 *In vitro* inhibition

In vitro MAO inhibition was determined for both ^{19}F-fluorodeprenyl-D_2 and ^{19}F-fluororasagiline-D_2 in an enzymatic assay with kynuramine as substrate. ^{19}F-Fluorodeprenyl-D_2 inhibited the MAO-B activity with an IC_{50} of 227 ± 36.8 nM and the MAO-A activity with an IC_{50} of >50 µM. Thus, deuteration decreased the IC_{50} towards MAO-B by ca. 7 times as compared to the non-deuterated fluorodeprenyl in the assay used. ^{19}F-Fluororasagiline-D_2 inhibited MAO-B with an IC_{50} = 173.0 ± 13.6 nM while inhibited MAO-A with an IC_{50} = 9.9 ± 1.1 µM.

4.4.3 PET in non-human primate

PET images and the time activity curves (TAC) of **47** and **50** uptake in a cynomolgus monkeys brain is shown in Figure 18-21. Both compounds cross the blood-brain barrier and bind rapidly. The brain uptake in a baseline condition was ~250% SUV and thus, in a similar range of other typical useful radioligands. The uptake was highest in the striatum and the thalamus followed by in the cortical areas and the cerebellum. This is consistent with the known distribution of *in vivo* MAO-B activity as previously reported for [^{11}C]deprenyl[81]. Both **47** and **50** showed faster wash-out from the brain and less accumulation in cortical and sub-cortical regions than compared to their non-deuterated analogues.

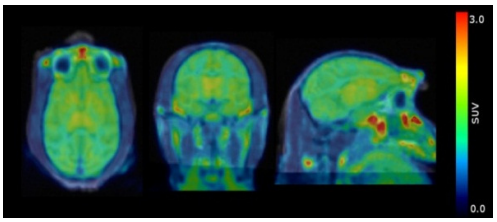

Figure 18. PET images of **47** baseline condition co-registered with MRI and averaged between 9 and 120 minutes in the horizontal (left), coronal (middle) and sagittal (right) projections.

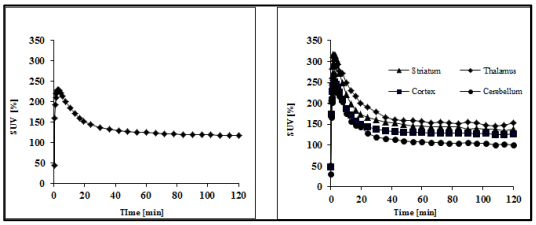

Figure 19. Brain uptake expressed as percent standardised uptake value (%SUV) after i.v. injection of **47**, in whole brain (left) and time activity curves in different brain regions (right).

Deuteration of **4c** lead to a significantly decreased uptake in the investigated brain regions. The effect of deuteration on the decrease in signal intensity for the [^{11}C]deprenyl–D_2 observed in healthy baboon and human brain regions was approximately 1.2 – 2.0[91]. In this study, we demonstrated a decrease in signal intensity of 5-6 times as a consequence of [^{18}F]fluorodeprenyl deuteration.

In the case of **50**, the signal intensity in target regions was up to 3 times lower than that in the case of [^{18}F]rasagiline (Figure 21). The reduced trapping rate of **50** enables an improved quantification of MAO-B activity and avoids blood flow limitation of delivery of the tracer, since it is known that a high trapping rate is responsible for an underestimation of the MAO-B signal in regions with high MAO-B activity.

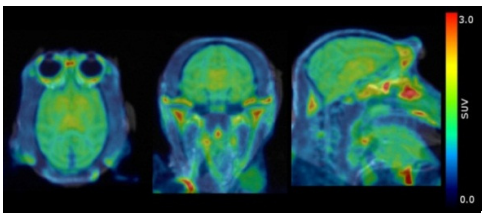

Figure 20. PET images of **50** baseline condition co-registered with MRI and averaged between 9 and 120 minutes in the horizontal (left), coronal (middle) and sagittal (right) projections.

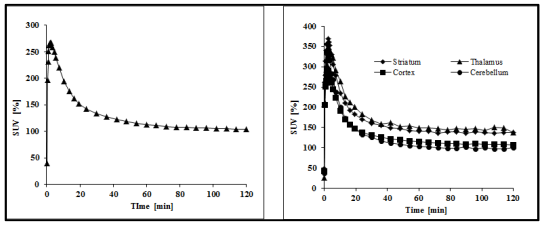

Figure 21. Brain uptake expressed as percent standardised uptake value (%SUV) after i.v. injection of **50**, in whole brain (left) and time activity curves in different brain regions (right).

The administration of 5 mg/kg of the MAO-B inhibitor *L*-deprenyl 30 minutes prior to the injection of **50** resulted in an approximately 50% decrease in the accumulation of the radioligand at 120 minutes p.i. in all brain regions (Figure 22 and 23).

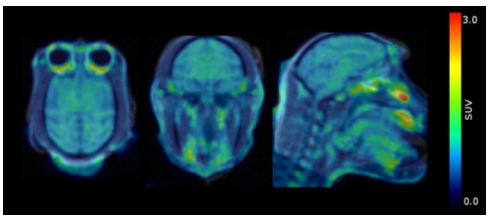

Figure 22. PET images of **50** co-registered with MRI and averaged between 9 and 120 minutes in the horizontal (left), coronal (middle) and sagittal (right) projections after pretreatment with *L*-deprenyl (5 mg/kg).

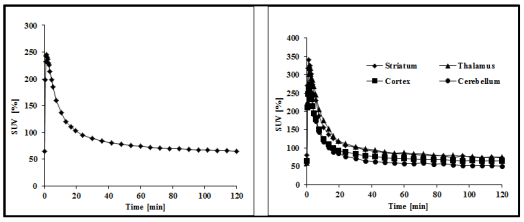

Figure 23. Brain uptake expressed as percent standardised uptake value (%SUV) after pretreatment with *L*-deprenyl (5 mg/kg). Time activity curves after i.v. injection of **50** in whole brain (left) and in different brain regions (right)

4.4.4 Radiometabolites measured in plasma

Radiometabolites of the radioligands measured in monkey plasma were analyzed by HPLC. Both radioligands showed a slower radiometabolism when compared to their non-deuterated analogues. Compound **47** showed similar pattern of metabolism as reported for both [^{11}C]deprenyl[128, 145] and [^{11}C]deprenyl-D_2[91].The two radiometabolites of [^{11}C]deprenyl have been extensively studied previously and have been found to correspond to [^{11}C]formic acid and its adducts, and [^{11}C]methamphetamine[130, 146]. Therefore the present compound will also more likely to have a radiometabolite which correspons to [^{18}F]fluoromethamphetamine.

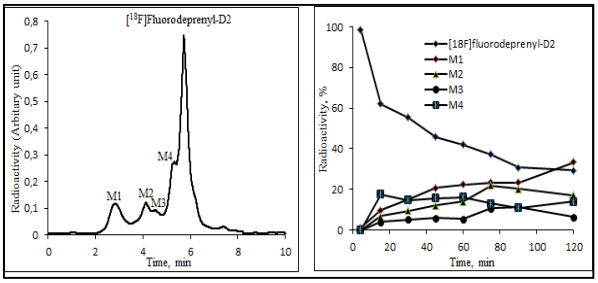

Figure 24. Radiometabolite analysis at 45 minutes p.i. of **47** (left) and during the time course of the PET measurements (right).

Compound **47** produced four radiometabolites with lower lipophilicity than the parent compound as judged from its short retention time on HPLC (Figure 24 left). At 15 minutes p.i. approximately 60% of the plasma radioactivity was unchanged **47**, decreasing to 45% at 45 minutes p.i. and 35% at 120 minutes p.i. (Figure 24 right).

For **50**, approximately 75% of the plasma radioactivity was unchanged parent compound at 15 minutes p.i., decreasing to 55% at 45 minutes p.i. and 35% at 120 minutes p.i. (Figure 25 right). Two radiometabolites, **a** and **b** (Figure 25 left) with lower lipophilicity than the parent compound were found. Radiometabolite **a** was more

abundant, representing approximately 35% of the plasma radioactivity at 120 minutes p.i. whereas **b** was less abundant with approximately 20% of the total plasma radioactivity at 120 minutes. As a consequence of deuteration we demonstrated that the metabolic stability of the parent compound was significantly increased. In addition, in the previous study with **23**, we observed a more lipophilic radiometabolite compared to the parent compound, which was eliminated after deuteration.

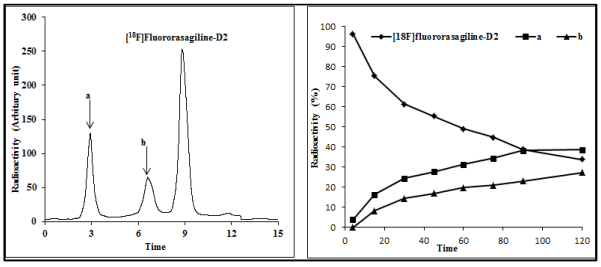

Figure 25. Radiometabolite analysis at 45 minutes p.i. of 50 (left) and during the time course of the PET measurements (right).

5 SUMMARY OF FINDINGS

Firstly, the two well established MAO-B inhibitors such as *L*-deprenyl and rasagiline were chosen to be labeled with fluorine-18. Fluorinated analogues of *L*-deprenyl were labeled with fluorine-18 at three different positions (**4a**, **4b** and **4c**). *In vitro* and *in vivo* studies demonstrated that only **4c** ([^{18}F]fluorodeprenyl) binds specifically to MAO-B rich regions of the brain and showed a similar kinetic behavior as previously reported for [^{11}C]deprenyl. Therefore, quantification of MAO-B using **4c** may be difficult because of fast irreversible binding to the enzyme renders the distribution of this radioligand in tissue limited by blood flow rather than the MAO-B enzyme concentration. On the other hand, with **23** ([^{18}F]fluororasagiline) we observed a continuing increase of the radioactivity in brain throughout the PET measurement that may indicate a blood-brain barrier penetrating radiometabolite that may in turn complicate a reliable quantification.

Secondly, three different fluorinated analogues of propargyl amines (**28**, **33** and **38**) were synthesized and tested for inhibition of MAO-B. Compounds **33** and **38** inhibited MAO-B in a range comparable to that of the therapeutically used compound deprenyl, and were chosen for fluorine-18 labeling for further investigation by ARG and PET. *In vitro* and *in vivo* studies demonstrated that only **38** binds specifically to MAO-B rich regions of the brain and showed similar kinetic behavior as previously reported for **23** i.e. a continuing increase of the radioactivity throughout the PET measurement.

Finally, in order to reduce the rate of radioligand trapping in human brain and thus, to improve its sensitivity as well as to reduce the radiometabolism measured in plasma, we synthesized fluorine-18 labeled deuterated fluorodeprenyl **47** and deuterated fluororasagiline **50** and examined them as novel PET radioligands for MAO-B. *In vitro* inhibition showed that both **47** and **50** inhibited MAO-B selectively. Both **47** and **50** were examined in the cynomolgus monkey brain where a high brain uptake was found (~250% SUV at 4 minutes) with higher amounts in the striatum and the thalamus compared to the cortex and the cerebellum as well as a faster wash-out from the brain. A radiometabolite study demonstrated that both **47** and **50** were more stable measured in monkey plasma as a consequence of deuteration when compared to the non-deuterated analogues.

These results together suggest that **47** and **50** are improved PET radioligands for imaging MAO-B.

6 FUTURE PERSPECTIVES AND CHALLENGES

Due to its central role in neurotransmitter metabolism, MAO-B represents an attractive drug target in the pharmacological therapy of neurodegenerative diseases. The MAO-B enzyme is upregulated in reactive astrocytes, giving rise to increased regional uptake of MAO-B inhibitors. Therefore, radiolabeled MAO-B inhibitors may be potential imaging biomarkers due to their affinity to the MAO-B enzyme for neurodegeneration. This thesis reported the development of two radiolabeled MAO-B inhibitors such as **47** ([^{18}F]fluorodeprenyl-D_2) and **50** ([^{18}F]fluororasagiline-D_2) effective for imaging MAO-B by PET.

Based on this work some future perspectives and specific challenges can be discussed for clinical use of **47** and **50** as PET radioligands.

Radiochemistry and purification

A PET radioligand, whether for clinical or preclinical use, should show a high level of chemical and radiochemical purity (typically >95%) also the radiosynthesis and purification should be performed as fast as possible. One step radiosynthesis is preferable for a PET radioligand to be clinically successful. Compound **47** was synthesized in one step simple nucleophilic substitution reaction. The final product is a mixture of two radiolabeled isomers which were purified by semi-preparative HPLC. It is quite complicated to purify the isomers by only solid phase extraction (SPE) alone, which is a common procedure for synthetic module that is not equipped with a HPLC for purification. Therefore, a future challenge will be to synthesize **47** as an isomerically pure compound. The synthesis of **50** was accomplished in two reaction steps. A future development will be to develop a one-step labeling procedure.

Analysis of radiometabolites

In a PET investigation, it is impossible to distinguish whether the radioactive uptake in the brain is dominated by signals from the parent radiotracer or its radiolabeled metabolites. After administration of both **47** and **50**, radiometabolite studies in monkey plasma, demonstrated the presence of several radiometabolites which were not extensively investigated and identified. Therefore, an additional future challenge would be a detailed analysis of BBB penetrating radiometabolites which can influence the quantification.

Binding kinetics

One potential disadvantage of using both **47** and **50** is the irreversible nature of their binding kinetics. As quantification of a reversible binding radioligand is generally preferable over an irreversible one, therefore, a final future prospective will be focused

on developing new PET radioligands for MAO-B with a reversible binding characteristic.

7 ACKNOWLEDGEMENTS

I would like to express my sincere gratitude and appreciation to all of them who have contributed directly or indirectly to make this thesis possible. I would specially like to thank:

Professor Christer Halldin, my supervisor, for accepting me as a PhD student in your group, your guidance and encouragement, enthusiasm, being available no matter where in the world you were as well as your ultimate support throughout these years. You have prepared me to meet new challenges in my future scientific career.

Dr. Lutz Lehmann, Dr. Georg Kettschau, Dr. Andrea Thiele and Dr. Tobias Heinrich for welcoming me at the Medicinal Chemistry lab of Bayer HealthCare AG and for your scientific discussion, constructive criticism and valuable comments during this work. Astrid Knop, for your technical support in the lab.

Associate Professor Andrea Varrone, for helping with PET data analysis and your positive comments as well as encouragement all the time. Professor Balazs Gulyas for helping with autoradiography and your valuable comments for writing manuscripts and Miklos Toth, for helping with PET data analysis.

All present and previous colleagues at the radiochemistry group at the Karolinska Institutet: Dr Anu J Airaksinen, for introducing me into the radiochemistry, Dr Magnus Schou for friendship and excellent scientific discussions about chemistry and radiochemistry, Dr. Obaidur Rahman for friendship and valuable discussions about science and life, Dr Jan Andersson for being a nice officemate for many years even though I was unable to teach you cricket, Kenneth Dahl and Phong Trong for your friendship and technical assistance.

A special thanks to Gudrun Nylen and Siv Eriksson for your excellent assistance with the monkey PET study and ARG respectively. Karin Zahir, for a great administrative assistance.

Arsalan Amir, Guennadi Jogolev, Dr. Jonas Bergström and Dr. Ryuji Nakao for excellent assistance with quality control and metabolite analysis in this thesis work. I thank all other members of the radiochemistry group who have made life at work easygoing: Dr. Zhisheng Jia, Carsten Steiger, Dr. Peter Johnström, Anna Sumic, Linda Bergman, Dr. Raisa Krasikova, Henrik Alfredeen, Dr. Nahid Amini, Dr. Vladimir Stepanov, Jacob Kihlström, Hanna Jacobson, Andreas Westermark, Nandor Kaposy, Mirkka Sarparanta, Dr. Sean Donohue, Dr. Stefan Martinsson and Dr. Fabienne Gourand.

All current and previous colleagues at the PET imaging group at the Karolinska Institutet: Dr. Sjoerd Finnema, Dr. Akihiro Takano, Dr. Anton Forsberg, Dr. Johan Lundberg, Dr. Katarina Varnäs, Dr. Per Kalsson, Dr. Jacqueline Borg, Dr. Simon Cervenka, Dr. Mikael Tiger, Dr. Magdalena Nord, Martin Schain, and Dr. Pavitra Kannan.

Karin Zahir, Urban Hansson, Karin Olsson, Göran Rosenqvist, Nils Sjöholm, Marianne Youssefi, Anncathrin Kallin, Johan Molin, Pia Schönbeck, Sofia Sjödin, Nina Knave for being a nice bunch of people.

Members of the radiochemistry group of the Karolinska pharmacy, Professor Sharon Stone-Elander, Dr. Jan-Olov Thorell, Erik Samen and Emma Jussing for smooth co-operation in the radiochemistry labs.

Professor Bengt Långström for giving the opportunity to do a project work in your group and Professor Stefan Sjöberg for introducing me to the Uppsala University and Professor Bengt Långström.

Professor M Mosihuzzaman, Professor Nilufar Nahar and Associate Professor Iqbal Rouf Mamun for giving me the opportunity to work with you and always inspiring me for research.

Friends: Emo, Kristofer, Dipu, Feku, Bernt, Shimul, Pamela, Kazi and Ratan bhai. Thanks for all support. Momin, thanks for friendship and all technical supports with computer.

My amazing family: Bapi, ma, dada and Biku. Thanks for your endless love and support, without which I wouldn't have come here today.

Finally I especially thank Jolly (Mahabuba Jahan) and Leeba for making a nice and happy family in Sweden and for your eternal support, inspiration and love. Jolly I would also like to thank for your positive and constructive criticisms/suggestions about chemistry and writing the thesis.

8 REFERENCES

1. Phelps M. E. PET: a biological imaging technique. *Neurochem Res* **1991,** 16, 929-40.
2. Welch M. J. and Redvanly C. S. Handbook of Radiopharmaceuticals: Radiochemistry and Application. *John Wiley & Sons Ltd, West Sussex, England* **2003**.
3. Ell P. J. and Gambhir S. S. Nuclear Medicine in Clinical Diagnosis and Treatment. *Elsevier Ltd* **2004,** 1.
4. Cassidy P. J. and Radda G. K. Molecular imaging perspectives. *J R Soc Interface* **2005,** 2, 133-44.
5. Eriksson L., Dahlbom M. and Widen L. Positron emission tomography--a new technique for studies of the central nervous system. *J Microsc* **1990,** 157, 305-33.
6. Cherry S. R. and Gambhir S. S. Use of positron emission tomography in animal research. *ILAR J* **2001,** 42, 219-32.
7. Basu S. and Alavi A. Unparalleled contribution of ^{18}F-FDG PET to medicine over 3 decades. *J Nucl Med* **2008,** 49, 17N-21N, 37N.
8. Morrish P. K., Rakshi J. S., Bailey D. L., Sawle G. V. and Brooks D. J. Measuring the rate of progression and estimating the preclinical period of Parkinson's disease with [^{18}F]dopa PET. *J Neuro Neuro Psy* **1998,** 64, 314-9.
9. Tolboom N., Yaqub M., van der Flier W. M., Boellaard R., Luurtsema G., Windhorst A. D., Barkhof F., Scheltens P., Lammertsma A. A. and van Berckel B. N. Detection of Alzheimer pathology in vivo using both [^{11}C]-PIB and ^{18}F-FDDNP PET. *J Nucl Med* **2009,** 50, 191-7.
10. Guadagno J. V., Warburton E. A., Jones P. S., Day D. J., Aigbirhio F. I., Fryer T. D., Harding S., Price C. J., Green H. A., Barret O., Gillard J. H. and Baron J. C. How affected is oxygen metabolism in DWI lesions?: A combined acute stroke PET-MR study. *Neurology* **2006,** 67, 824-9.
11. Gee A. D. Neuropharmacology and drug development. *Br Med Bull* **2003,** 65, 169-77.
12. Halldin C., Gulyas B. and Farde L. PET studies with carbon-11 radioligands in neuropsychopharmacological drug development. *Curr Pharm Des* **2001,** 7, 1907-29.
13. Passchier J., Gee A., Willemsen A., Vaalburg W. and van Waarde A. Measuring drug-related receptor occupancy with positron emission tomography. *Methods* **2002,** 27, 278-86.
14. Gatley S. J., Volkow N. D., Fowler J. S., Ding Y. S., Logan J., Wang G. J. and Gifford A. N. Positron emission tomography and its use to image the occupancy of drug binding sites. *Drug Development Research* **2003,** 59, 194-207.
15. Farde L. and Hall H. Positron emission tomography--examination of chemical transmission in the living human brain. Development of radioligands. *Arzneimittelforschung* **1992,** 42, 260-4.
16. Lee C. M. and Farde L. Using positron emission tomography to facilitate CNS drug development. *Trends Pharmacol Sci* **2006,** 27, 310-6.

17. Bergstrom M., Grahnen A. and Langstrom B. Positron emission tomography microdosing: a new concept with application in tracer and early clinical drug development. *Eur J Clin Pharmacol* **2003,** 59, 357-66.
18. Molecular imaging that will bring about a revolution in diagnosis and drug discovery. *Riken Research* *http://www.rikenresearch.riken.jp/eng/frontline/5656.html* **2008**.
19. Halldin C., Gulyas B., Langer O. and Farde L. Brain radioligands--state of the art and new trends. *Q J Nucl Med* **2001,** 45, 139-52.
20. Pike V. W. PET radiotracers: crossing the blood-brain barrier and surviving metabolism. *Trends Pharmacol Sci* **2009,** 30, 431-40.
21. Laruelle M., Slifstein M. and Huang Y. Relationships between radiotracer properties and image quality in molecular imaging of the brain with positron emission tomography. *Mol Imaging Biol* **2003,** 5, 363-75.
22. Waterhouse R. N. Determination of lipophilicity and its use as a predictor of blood-brain barrier penetration of molecular imaging agents. *Mol Imaging Biol* **2003,** 5, 376-89.
23. Pike V. W. Positron-emitting radioligands for studies in vivo-probes for human psychopharmacology. *J Psychopharmacol* **1993,** 7, 139-58.
24. Elsinga P. H. Radiopharmaceutical chemistry for positron emission tomography. *Methods* **2002,** 27, 208-17.
25. Wong D. F. and Pomper M. G. Predicting the success of a radiopharmaceutical for in vivo imaging of central nervous system neuroreceptor systems. *Mol Imaging Biol* **2003,** 5, 350-62.
26. Dickson C. J., Gee A. D., Bennacef I., Gould I. R. and Rosso L. Further evaluation of quantum chemical methods for the prediction of non-specific binding of positron emission tomography tracers. *Phys Chem Chem Phys* **2011,** 13, 21552-7.
27. Dishino D. D., Welch M. J., Kilbourn M. R. and Raichle M. E. Relationship between lipophilicity and brain extraction of C-11-labeled radiopharmaceuticals. *J Nucl Med* **1983,** 24, 1030-8.
28. Moerlein S. M., Laufer P. and Stocklin G. Effect of lipophilicity on the in vivo localization of radiolabelled spiperone analogues. *Int J Nucl Med Biol* **1985,** 12, 353-6.
29. Seddon A. M., Casey D., Law R. V., Gee A., Templer R. H. and Ces O. Drug interactions with lipid membranes. *Chem Soc Rev* **2009,** 38, 2509-19.
30. Patel S. and Gibson R. In vivo site-directed radiotracers: a mini-review. *Nucl Med Biol* **2008,** 35, 805-15.
31. Elsinga P. H., Hendrikse N. H., Bart J., Vaalburg W. and van Waarde A. PET Studies on P-glycoprotein function in the blood-brain barrier: how it affects uptake and binding of drugs within the CNS. *Curr Pharm Des* **2004,** 10, 1493-503.
32. Kannan P., John C., Zoghbi S. S., Halldin C., Gottesman M. M., Innis R. B. and Hall M. D. Imaging the function of P-glycoprotein with radiotracers: pharmacokinetics and in vivo applications. *Clin Pharmacol Ther* **2009,** 86, 368-77.
33. Raub T. J. P-glycoprotein recognition of substrates and circumvention through rational drug design. *Mol Pharm* **2006,** 3, 3-25.

34. Olsson H., Halldin C. and Farde L. Differentiation of extrastriatal dopamine D2 receptor density and affinity in the human brain using PET. *Neuroimage* **2004,** 22, 794-803.

35. Bergman J., Eskola O., Lehikoinen P. and Solin O. Automated synthesis and purification of [^{18}F]bromofluoromethane at high specific radioactivity. *Appl Radiat Isot* **2001,** 54, 927-33.

36. Lapi S. E. and Welch M. J. A historical perspective on the specific activity of radiopharmaceuticals: what have we learned in the 35 years of the ISRC? *Nucl Med Biol* **2012,** 39, 601-8.

37. Fortt R. and Gee A. Microfluidics: a golden opportunity for positron emission tomography? *Future Med Chem* **2013,** 5, 241-4.

38. Lu S. Y. and Pike V. W. Micro-reactors for PET tracer labeling. *Ernst Schering Res Found Workshop* **2007**, 271-87.

39. Langstrom B., Itsenko O. and Rahman O. C-11 Carbon monoxide, a versatile and useful precursor in labelling chemistry for PET ligand development. *Journal of Labelled Compounds & Radiopharmaceuticals* **2007,** 50, 794-810.

40. Dahl K., Schou M., Amini N. and Halldin C. Palladium-Mediated C-11 Carbonylation at Atmospheric Pressure: A General Method Using Xantphos as Supporting Ligand. *European Journal of Organic Chemistry* **2013**, 1228-1231.

41. Halldin C., Swahn C. G., Farde L. and Sedvall G. Radioligand disposition and metabolism. *Kluwer Academic Publishers* **1995**, 55.

42. Chitneni S. K., Serdons K., Evens N., Fonge H., Celen S., Deroose C. M., Debyser Z., Mortelmans L., Verbruggen A. M. and Bormans G. M. Efficient purification and metabolite analysis of radiotracers using high-performance liquid chromatography and on-line solid-phase extraction. *J Chromatography A* **2008,** 1189, 323-331.

43. Osman S., Lundkvist C., Pike V. W., Halldin C., McCarron J. A., Swahn C. G., Farde L., Ginovart N., Luthra S. K., Gunn R. N., Bench C. J., Sargent P. A. and Grasby P. M. Characterisation of the appearance of radioactive metabolites in monkey and human plasma from the 5-HT1A receptor radioligand, [^{11}C]WAY-100635--explanation of high signal contrast in PET and an aid to biomathematical modelling. *Nucl Med Biol* **1998,** 25, 215-23.

44. Hare M. L. Tyramine oxidase: A new enzyme system in liver. *Biochem J* **1928,** 22, 968-79.

45. Blaschko H., Richter D. and Schlossmann H. The inactivation of adrenaline. *J Physiol* **1937,** 90, 1-17.

46. Zeller E. A. Über den enzymatischen Abbau von Histamin und Diaminen. 2. Mitteilung. *Helvetica Chimica Acta* **1938,** 21, 880-890.

47. Singer T. P. and Ramsay R. R. Flauoprotein structure and mechanism 2. Monoamine oxidases: old friends hold many surprises. *FASEB J* **1995,** 9, 605-10.

48. Bach A. W. J., Lan N. C., Bruke D. J., Abell C. W., Bembenek M. E., Kwan S. W., Seeburg P. H. and Shih J. C. Molecular-cloning of human monoamine oxidase-A and oxidase-B (MAO-A and MAO-B). *Faseb Journal* **1988,** 2, A1733-A1733.

49. Tipton K. F., Boyce S., O'Sullivan J., Davey G. P. and Healy J. Monoamine oxidases: Certainties and uncertainties. *Curr Med Chem* **2004,** 11, 1965-1982.
50. Smith M. A., Rottkamp C. A., Nunomura A., Raina A. K. and Perry G. Oxidative stress in Alzheimer's disease. *Biochim Biophys Acta* **2000,** 1502, 139-44.
51. Su A. I., Wiltshire T., Batalov S., Lapp H., Ching K. A., Block D., Zhang J., Soden R., Hayakawa M., Kreiman G., Cooke M. P., Walker J. R. and Hogenesch J. B. A gene atlas of the mouse and human protein-encoding transcriptomes. *Proc Natl Acad Sci U S A* **2004,** 101, 6062-7.
52. Levitt P., Pintar J. E. and Breakefield X. O. Immunocytochemical demonstration of monoamine oxidase B in brain astrocytes and serotonergic neurons. *Proc Natl Acad Sci U S A* **1982,** 79, 6385-9.
53. Shih J. C., Chen K. and Ridd M. J. Monoamine oxidase: from genes to behavior. *Annu Rev Neurosci* **1999,** 22, 197-217.
54. Nakamura S., Kawamata T., Akiguchi I., Kameyama M., Nakamura N. and Kimura H. Expression of monoamine oxidase B activity in astrocytes of senile plaques. *Acta Neuropathol* **1990,** 80, 419-25.
55. Cesura A. M. and Pletscher A. The new generation of monoamine oxidase inhibitors. *Prog Drug Res* **1992,** 38, 171-297.
56. Oreland L., Arai Y., Stenstrom A. and Fowler C. J. Monoamine oxidase activity and localisation in the brain and the activity in relation to psychiatric disorders. *Mod Probl Pharmacopsychiatry* **1983,** 19, 246-54.
57. Squires R. F. Multiple forms of monoamine oxidase in intact mitochondria as characterized by selective inhibitors and thermal stability: a comparison of eight mammalian species. *Adv Biochem Psychopharmacol* **1972,** 5, 355-70.
58. Yamada M. and Yasuhara H. Clinical pharmacology of MAO inhibitors: safety and future. *Neurotoxicology* **2004,** 25, 215-21.
59. Fariello R. G. and Lieberman A. Present and future approaches to Parkinson disease: from molecular insights to new therapeutic avenues. *Neurology* **2006,** 67, S1-4.
60. Youdim M. B. H. and Bakhle Y. S. Monoamine oxidase: isoforms and inhibitors in Parkinson's disease and depressive illness. *British J Pharm* **2006,** 147, S287-S296.
61. Bortolato M., Chen K. and Shih J. C. Monoamine oxidase inactivation: from pathophysiology to therapeutics. *Adv Drug Deliv Rev* **2008,** 60, 1527-33.
62. Andrews J. M. and Nemeroff C. B. Contemporary management of depression. *Am J Med* **1994,** 97, S24-S32.
63. Drukarch B. and van Muiswinkel F. L. Drug treatment of Parkinson's disease - Time for phase II. *Biochemical Pharmacology* **2000,** 59, 1023-1031.
64. Holtzheimer P. E. and Nemeroff C. B. Emerging treatments for depression. *Expert Opinion on Pharmacotherapy* **2006,** 7, 2323-2339.
65. Ramsay R. R. Substrate regulation of monoamine oxidases. *J Neural Transm Suppl* **1998,** 52, 139-47.

66. Abeles R. H. Suicide enzyme inactivators. *Basic Life Sci* **1983,** 25, 287-305.

67. Knoll J., Ecseri Z., Kelemen K., Nievel J. and Knoll B. Phenylisopropylmethylpropinylamine (E-250), a new spectrum psychic energizer. *Arch Int Pharmacodyn Ther* **1965,** 155, 154-64.

68. Magyar K., Vizi E. S., Ecseri Z. and Knoll J. Comparative pharmacological analysis of the optical isomers of phenyl-isopropyl-methyl-propinylamine (E-250). *Acta Physiol Acad Sci Hung* **1967,** 32, 377-87.

69. Finberg J. P., Lamensdorf I., Commissiong J. W. and Youdim M. B. Pharmacology and neuroprotective properties of rasagiline. *J Neural Transm Suppl* **1996,** 48, 95-101.

70. Palfreyman M. G., McDonald I. A., Bey P., Danzin C., Zreika M. and Cremer G. Haloallylamine inhibitors of MAO and SSAO and their therapeutic potential. *J Neural Transm Suppl* **1994,** 41, 407-14.

71. Da Prada M., Kettler R., Keller H. H. and Burkard W. P. Short-lasting and reversible inhibition of monoamine oxidase-A by moclobemide. *Acta Psychiatr Scand Suppl* **1990,** 360, 103-5.

72. Bench C. J., Price G. W., Lammertsma A. A., Cremer J. C., Luthra S. K., Turton D., Dolan R. J., Kettler R., Dingemanse J., Da Prada M. and et al. Measurement of human cerebral monoamine oxidase type B (MAO-B) activity with positron emission tomography (PET): a dose ranging study with the reversible inhibitor Ro 19-6327. *Eur J Clin Pharmacol* **1991,** 40, 169-73.

73. Lebreton L., Curet O., Gueddari S., Mazouz F., Bernard S., Burstein C. and Milcent R. Selective and potent monoamine oxidase type B inhibitors: 2-substituted 5-aryltetrazole derivatives. *J Med Chem* **1995,** 38, 4786-92.

74. Truong D. D., Galloway M. P., Pezzoli G., Jamrozik Z. and Fahn S. Milacemide increases 5-hydroxytryptamine and dopamine levels in rat brain--possible mechanisms of milacemide antimyoclonic property in the p,p'-DDT-induced myoclonus. *Pharmacol Biochem Behav* **1989,** 32, 993-1001.

75. Santillo A. F., Gambini J. P., Lannfelt L., Langstrom B., Ulla-Marja L., Kilander L. and Engler H. In vivo imaging of astrocytosis in Alzheimer's disease: an [^{11}C]-*L*-deuteriodeprenyl and PIB PET study. *Eur J Nucl Med Mol Imaging* **2011,** 38, 2202-8.

76. Bergstrom M., Kumlien E., Lilja A., Tyrefors N., Westerberg G. and Langstrom B. Temporal lobe epilepsy visualized with PET with [^{11}C]L-deuterium-deprenyl--analysis of kinetic data. *Acta Neurol Scand* **1998,** 98, 224-31.

77. Fowler J. S., Logan J., Volkow N. D., Wang G. J., MacGregor R. R. and Ding Y. S. Monoamine oxidase: radiotracer development and human studies. *Methods* **2002,** 27, 263-277.

78. Fowler J. S., Logan J., Volkow N. D. and Wang G. J. Translational neuroimaging: positron emission tomography studies of monoamine oxidase. *Mol Imaging Biol* **2005,** 7, 377-87.

79. Holland J. P., Cumming P. and Vasdev N. PET radiopharmaceuticals for probing enzymes in the brain. *Am J Nucl Med Mol Imaging* **2013,** 3, 194-216.

80. MacGregor R. R., Halldin C., Fowler J. S., Wolf A. P., Arnett C. D., Langstrom B. and Alexoff D. Selective, irreversible in vivo binding of [^{11}C]clorgyline and [^{11}C]-L-deprenyl in mice: potential for measurement of functional monoamine oxidase activity in brain using positron emission tomography. *Biochem Pharmacol* **1985,** 34, 3207-10.

81. Fowler J. S., Macgregor R. R., Wolf A. P., Arnett C. D., Dewey S. L., Schlyer D., Christman D., Logan J., Smith M., Sachs H., Aquilonius S. M., Bjurling P., Halldin C., Hartvig P., Leenders K. L., Lundqvist H., Oreland L., Stalnacke C. G. and Langstrom B. Mapping human-brain monoamine oxidase-A and oxidase-B with C-11 labeled suicide inactivators and PET. *Science* **1987,** 235, 481-485.

82. Ishiwata K., Ido T., Yanai K., Kawashima K., Miura Y., Monma M., Watanuki S., Takahashi T. and Iwata R. Biodistribution of a positron-emitting suicide inactivator of monoamine oxidase, carbon-11 pargyline, in mice and a rabbit. *J Nucl Med* **1985,** 26, 630-6.

83. Hirvonen J., Kailajarvi M., Haltia T., Koskimies S., Nagren K., Virsu P., Oikonen V., Sipila H., Ruokoniemi P., Virtanen K., Scheinin M. and Rinne J. O. Assessment of MAO-B occupancy in the brain with PET and [^{11}C]-L-deprenyl-D2: a dose-finding study with a novel MAO-B inhibitor, EVT 301. *Clin Pharmacol Ther* **2009,** 85, 506-12.

84. Carter S. F., Scholl M., Almkvist O., Wall A., Engler H., Langstrom B. and Nordberg A. Evidence for astrocytosis in prodromal Alzheimer disease provided by [^{11}C]-deuterium-L-deprenyl: a multitracer PET paradigm combining [^{11}C]-Pittsburgh compound B and ^{18}F-FDG. *J Nucl Med* **2012,** 53, 37-46.

85. Hirata M., Kagawa S., Yoshimoto M. and Ohmomo Y. Synthesis and characterization of radioiodinated MD-230254: a new ligand for potential imaging of monoamine oxidase B activity by single photon emission computed tomography. *Chem Pharm Bull (Tokyo)* **2002,** 50, 609-14.

86. Plenevaux A., Fowler J. S., Dewey S. L., Wolf A. P. and Guillaume M. The synthesis of no-carrier-added DL-4-[^{18}F]fluorodeprenyl via the nucleophilic aromatic substitution reaction. *Int J Rad Appl Instrum A* **1991,** 42, 121-7.

87. Mukherjee J., Yang Z. Y. and Lew R. N-(6-^{18}F-fluorohexyl)-N-methylpropargylamine: a fluorine-18-labeled monoamine oxidase B inhibitor for potential use in PET studies. *Nucl Med Biol* **1999,** 26, 111-6.

88. Saba W., Valette H., Peyronneau M. A., Bramoulle Y., Coulon C., Curet O., George P., Dolle F. and Bottlaender M. [^{11}C]SL25.1188, a new reversible radioligand to study the monoamine oxidase type B with PET: preclinical characterisation in nonhuman primate. *Synapse* **2010,** 64, 61-9.

89. Blauenstein P., Remy N., Buck A., Ametamey S., Haberli M. and Schubiger P. A. In vivo properties of N-(2-aminoethyl)-5-halogeno-2-pyridinecarboxamide ^{18}F- and ^{123}I-labelled reversible inhibitors of monoamine oxidase B. *Nucl Med Biol* **1998,** 25, 47-52.

90. Beer H. F., Frey L. D., Haberli M. and Schubiger P. A. [^{123}I/^{18}F] N-(2-aminoethyl)-5-halogeno-2-pyridinecarbox-amides, site specific tracers for MAO-B mapping with SPECT and PET. *Nucl Med Biol* **1995,** 22, 999-1004.

91. Fowler J. S., Wang G. J., Logan J., Xie S., Volkow N. D., MacGregor R. R., Schlyer D. J., Pappas N., Alexoff D. L., Patlak C. and et al. Selective reduction of radiotracer trapping by deuterium substitution: comparison of carbon-11-L-deprenyl and carbon-11-deprenyl-D2 for MAO B mapping. *J Nucl Med* **1995,** 36, 1255-62.

92. Halldin C., Bjurling P., Stalnacke C. G., Jossan S. S., Oreland L. and Langstrom B. [^{11}C]labelling of dimethylphenethylamine in two different positions and biodistribution studies. *Int J Rad Appl Instrum A* **1989,** 40, 557-60.

93. Park B. K. and Kitteringham N. R. Effects of fluorine substitution on drug metabolism: pharmacological and toxicological implications. *Drug Metab Rev* **1994,** 26, 605-43.

94. Le Bars D. Fluorine-18 and medical imaging: Radiopharmaceuticals for positron emission tomography. *J Fluor Chem* **2006,** 127, 1488-1493.

95. Hagmann W. K. The many roles for fluorine in medicinal chemistry. *J Med Chem* **2008,** 51, 4359-69.

96. Schlyer D. J. Production of radionuclides in accelerators, in Welch MJ, Redvanley CS (eds): Handbook of Radiopharmaceuticals, Radiochemistry and Applications. *New York, John Wiley & Sons Inc* **2003**.

97. Bergman J. and Solin O. Fluorine-18-labeled fluorine gas for synthesis of tracer molecules. *Nucl Med Biol* **1997,** 24, 677-83.

98. Teare H., Robins E. G., Kirjavainen A., Forsback S., Sandford G., Solin O., Luthra S. K. and Gouverneur V. Radiosynthesis and evaluation of [^{18}F]Selectfluor bis(triflate). *Angew Chem Int Ed Engl* **2010,** 49, 6821-4.

99. Satyamurthy N., Bida G. T., Phelps M. E. and Barrio J. R. N-[^{18}F]fluoro-N-alkylsulfonamides: novel reagents for mild and regioselective radiofluorination. *Int J Rad Appl Instrum A* **1990,** 41, 733-8.

100. Gallagher B. M., Ansari A., Atkins H., Casella V., Christman D. R., Fowler J. S., Ido T., MacGregor R. R., Som P., Wan C. N., Wolf A. P., Kuhl D. E. and Reivich M. Radiopharmaceuticals XXVII. ^{18}F-labeled 2-deoxy-2-fluoro-d-glucose as a radiopharmaceutical for measuring regional myocardial glucose metabolism in vivo: tissue distribution and imaging studies in animals. *J Nucl Med* **1977,** 18, 990-6.

101. Levy S., Elmaleh D. R. and Livni E. A new method using anhydrous [^{18}F]fluoride to radiolabel 2-[^{18}F]fluoro-2-deoxy-D-glucose. *J Nucl Med* **1982,** 23, 918-22.

102. Namavari M., Bishop A., Satyamurthy N., Bida G. and Barrio J. R. Regioselective radiofluorodestannylation with [^{18}F]F2 and [^{18}F]CH3COOF: a high yield synthesis of 6-[^{18}F]Fluoro-L-dopa. *Int J Rad Appl Instrum A* **1992,** 43, 989-96.

103. Schlyer D. J., Firouzbakht M. L. and Wolf A. P. Impurities in the [^{18}O]water target and their effect on the yield of an aromatic displacement reaction with [^{18}F]fluoride. *Appl Radiat Isot* **1993,** 44, 1459-65.

104. Schlyer D. J. PET tracers and radiochemistry. *Ann Acad Med Singapore* **2004,** 33, 146-54.

105. Gomzina N. A., Vasil'ev D. A. and Krasikova R. N. Optimization of Automated Synthesis of 2-[^{18}F]Fluoro-2-deoxy-D-glucose Involving Base Hydrolysis. *Radiochemistry* **2002,** 44, 403-409.

106. Block D., Klatte B., Knochel A., Beckmann R. and Holm U. NCA F-18 labeling of aliphatic compounds in high yields via aminopolyether-supported nucleophilic substitution. *J Label Com Radio* **1986,** 23, 467-477.

107. Hamacher K., Coenen H. H. and Stocklin G. Efficient stereospecific synthesis of no-carrier-added 2-[^{18}F]-fluoro-2-deoxy-D-glucose using aminopolyether supported nucleophilic substitution. *J Nucl Med* **1986,** 27, 235-8.

108. Kim D. W., Ahn D. S., Oh Y. H., Lee S., Kil H. S., Oh S. J., Lee S. J., Kim J. S., Ryu J. S., Moon D. H. and Chi D. Y. A new class of SN2 reactions catalyzed by protic solvents: Facile fluorination for isotopic labeling of diagnostic molecules. *J Am Chem Soc* **2006,** 128, 16394-7.

109. Kim D. W., Jeong H. J., Lim S. T., Sohn M. H., Katzenellenbogen J. A. and Chi D. Y. Facile nucleophilic fluorination reactions using tert-alcohols as a reaction medium: significantly enhanced reactivity of alkali metal fluorides and improved selectivity. *J Org Chem* **2008,** 73, 957-62.

110. Lee S. J., Oh S. J., Chi D. Y., Kang S. H., Kil H. S., Kim J. S. and Moon D. H. One-step high-radiochemical-yield synthesis of [^{18}F]FP-CIT using a protic solvent system. *Nucl Med Biol* **2007,** 34, 345-51.

111. Ametamey S. M., Honer M. and Schubiger P. A. Molecular imaging with PET. *Chem Rev* **2008,** 108, 1501-16.

112. Kilbourn M. R. Fluorine-18 labeling of radiopharmaceuticals. *Nuclear Science Series* **1990,** NAS-NS3203, National Academy Press, Washington, D.C.

113. Dolle F. Fluorine-18-labelled fluoropyridines: Advances in radiopharmaceutical design. *Current Pharmaceutical Design* **2005,** 11, 3221-3235.

114. Angelini G., Speranza M., Wolf A. P. and Shiue C. Y. Nucleophilic aromatic-substitution of activated cationic groups by F-18-labeled fluoride - A useful route to no-carrier-added (NCA) F-18-labeled aryl fluorides. *J Fluor Chem* **1985,** 27, 177-191.

115. Carroll M. A., Pike V. W. and Widdowson D. A. New synthesis of diaryliodonium sulfonates from arylboronic acids. *Tetrahedron Letters* **2000,** 41, 5393-5396.

116. Weissbach H., Smith T. E., Daly J. W., Witkop B. and Udenfriend S. A rapid spectrophotometric assay of mono-amine oxidase based on the rate of disappearance of kynuramine. *J Biol Chem* **1960,** 235, 1160-3.

117. Hall H., Halldin C., Farde L. and Sedvall G. Whole hemisphere autoradiography of the postmortem human brain. *Nucl Med Biol* **1998,** 25, 715-9.

118. Schou M., Halldin C., Pike V. W., Mozley P. D., Dobson D., Innis R. B., Farde L. and Hall H. Post-mortem human brain autoradiography of the norepinephrine transporter using (S,S)-[^{18}F]FMeNER-D2. *Eur Neuropsychopharmacol* **2005,** 15, 517-20.

119. Gulyas B., Makkai B., Kasa P., Gulya K., Bakota L., Varszegi S., Beliczai Z., Andersson J., Csiba L., Thiele A., Dyrks T., Suhara T., Suzuki K., Higuchi M. and Halldin C. A comparative autoradiography study in post mortem whole hemisphere human brain slices taken from Alzheimer patients and age-matched controls using two radiolabelled DAA1106 analogues with high affinity to the

peripheral benzodiazepine receptor (PBR) system. *Neurochemistry International* **2009,** 54, 28-36.

120. Clark J. D., Gebhart G. F., Gonder J. C., Keeling M. E. and Kohn D. F. Special Report: The 1996 Guide for the Care and Use of Laboratory Animals. *ILAR J* **1997,** 38, 41-48.

121. Karlsson P., Farde L., Halldin C., Swahn C. G., Sedvall G., Foged C., Hansen K. T. and Skrumsager B. PET examination of [^{11}C]NNC 687 and [^{11}C]NNC 756 as new radioligands for the D1-dopamine receptor. *Psychopharmacology (Berl)* **1993,** 113, 149-56.

122. Varrone A., Sjoholm N., Eriksson L., Gulyas B., Halldin C. and Farde L. Advancement in PET quantification using 3D-OP-OSEM point spread function reconstruction with the HRRT. *Eur J Nucl Med Mol Imaging* **2009,** 36, 1639-50.

123. Knoll J. Critical role of MAO inhibition in Parkinson's disease. *Adv Neurol* **1987,** 45, 107-10.

124. Fowler C. J. and Ross S. B. Selective inhibitors of monoamine oxidase A and B: biochemical, pharmacological, and clinical properties. *Med Res Rev* **1984,** 4, 323-58.

125. Effects of tocopherol and deprenyl on the progression of disability in early Parkinson's disease. The Parkinson Study Group. *N Engl J Med* **1993,** 328, 176-83.

126. Fowler J. S., Logan J., Wang G. J., Volkow N. D., Telang F., Ding Y. S., Shea C., Garza V., Xu Y. W., Li Z. H., Alexoff D., Vaska P., Ferrieri R., Schlyer D., Zhu W. and Gatley S. J. Comparison of the binding of the irreversible monoamine oxidase tracers, [^{11}C]clorgyline and [^{11}C]*l*-deprenyl in brain and peripheral organs in humans. *Nuclear Medicine and Biology* **2004,** 31, 313-319.

127. Metro T. X., Appenzeller J., Pardo D. G. and Cossy J. Highly enantioselective synthesis of beta-amino alcohols. *Org Lett* **2006,** 8, 3509-3512.

128. Arnett C. D., Fowler J. S., MacGregor R. R., Schlyer D. J., Wolf A. P., Langstrom B. and Halldin C. Turnover of brain monoamine oxidase measured in vivo by positron emission tomography using L-[^{11}C]deprenyl. *J Neurochem* **1987,** 49, 522-7.

129. Shin H. S. Metabolism of selegiline in humans - Identification, excretion, and stereochemistry of urine metabolites. *Drug Metabolism and Disposition* **1997,** 25, 657-662.

130. Cumming P., Yokoi F., Chen A., Deep P., Dagher A., Reutens D., Kapczinski F., Wong D. F. and Gjedde A. Pharmacokinetics of radiotracers in human plasma during positron emission tomography. *Synapse* **1999,** 34, 124-34.

131. Reynolds G. P., Elsworth J. D., Blau K., Sandler M., Lees A. J. and Stern G. M. Deprenyl is metabolized to methamphetamine and amphetamine in man. *Br J Clin Pharmacol* **1978,** 6, 542-4.

132. Yoshida T., Yamada Y., Yamamoto T. and Kuroiwa Y. Metabolism of deprenyl, a selective monoamine oxidase (MAO) B inhibitor in rat: relationship of metabolism to MAO-B inhibitory potency. *Xenobiotica* **1986,** 16, 129-36.

133. Stocchi F., Vacca L., Grassini P., De Pandis M. F., Battaglia G., Cattaneo C. and Fariello R. G. Symptom relief in Parkinson disease by safinamide: Biochemical

and clinical evidence of efficacy beyond MAO-B inhibition. *Neurology* **2006,** 67, S24-9.

134. Bar Am O., Amit T. and Youdim M. B. Contrasting neuroprotective and neurotoxic actions of respective metabolites of anti-Parkinson drugs rasagiline and selegiline. *Neurosci Lett* **2004,** 355, 169-72.

135. Bar-Am O., Amit T. and Youdim M. B. Aminoindan and hydroxyaminoindan, metabolites of rasagiline and ladostigil, respectively, exert neuroprotective properties in vitro. *J Neurochem* **2007,** 103, 500-8.

136. Couty F., Durrat F. and Prim D. Expeditive synthesis of homochiral fused tri- and tetrazoles-piperazines from beta-amino alcohols. *Tetrahedron Letters* **2004,** 45, 3725-3728.

137. Bowen R. D., Harrison A. G. and Reiner E. J. Ion-dipole complexes in the unimolecular reactions of isolated organic ions-effect of N-methylation on olefin and amine loss from protected aliphatic-amines. *Journal of the Chemical Society-Perkin Transactions 2* **1988**, 1009-1013.

138. Melander L. and Saunders W. H. J. Reaction Rates of Isotopic Molecules. *John Wiley and Sons, New York* **1980**.

139. Yu P. H., Barclay S., Davis B. and Boulton A. A. Deuterium isotope effects on the enzymatic oxidative deamination of trace amines. *Biochem Pharmacol* **1981,** 30, 3089-94.

140. Fowler J. S., Wolf A. P., MacGregor R. R., Dewey S. L., Logan J., Schlyer D. J. and Langstrom B. Mechanistic positron emission tomography studies: demonstration of a deuterium isotope effect in the monoamine oxidase-catalyzed binding of [^{11}C]L-deprenyl in living baboon brain. *J Neurochem* **1988,** 51, 1524-34.

141. Logan J., Fowler J. S., Volkow N. D., Wang G. J., MacGregor R. R. and Shea C. Reproducibility of repeated measures of deuterium substituted [^{11}C]L-deprenyl ([^{11}C]L-deprenyl-D2) binding in the human brain. *Nucl Med Biol* **2000,** 27, 43-9.

142. Davister M. and Locht R. The dissociative ionisation of C2H2 and C2D2-the CH(CD) (+) dissociation channel – the H(D)C-C(D)H binding-energy. *Chemical Physics* **1995,** 191, 333-346.

143. Fowler J. S., Wang G. J., Logan J., Xie S., Volkow N. D., Macgregor R. R., Schlyer D. J., Pappas N., Alexoff D. L., Patlak C. and Wolf A. P. Selective reduction of radiotracer trapping by deuterium substitution – comparison of carbon-11-L-deprenyl and carbon-11-L-deprenyl-D2 for MAO-B mapping *J Nucl Med* **1995,** 36, 1255-1262.

144. Johansson A., Engler H., Blomquist G., Scott B., Wall A., Aquilonius S. M., Langstrom B. and Askmark H. Evidence for astrocytosis in ALS demonstrated by [^{11}C](L)-deprenyl-D2 PET. *J Neurol Sci* **2007,** 255, 17-22.

145. Dolle F., Bramoulle Y., Hinnen F. and Fowler J. S. Efficient synthesis and formulation of (R)-(-)- C-11 Deprenyl, a selective radioligand for the quantification of MAO-B activity using PET. *J Label Com Radio* **2002,** 45, 803-811.

146. Kalasz H., Bartok T., Komoroczy R., Szoko E., Haberle D., Kiss J. P., Hennings E. C. P., Magyar K. and Furst S. Analysis of deprenyl metabolites in the rat brain using HPLC-ESMS. *Curr Med Chem* **1999,** 6, 271-278.